Taherzadeh-Soureshjani and Chehelgerdi
Cancer Nano (2020) 11:11
https://doi.org/10.1186/s12645-020-00066-4

Cancer Nanotechnology

RESEARCH

Open Access

Algae-meditated route to cuprous oxide (Cu_2O) nanoparticle: differential expression profile of *MALAT1* and *GAS5* LncRNAs and cytotoxic effect in human breast cancer

Parisa Taherzadeh-Soureshjani and Mohammad Chehelgerdi*

*Correspondence:
Chehelgerdi1992@gmail.com
Young Researchers and Elite Club, Shahrekord Branch, Islamic Azad University, Shahrekord, Iran

Abstract

Background: Breast cancer (BC), as the most widely recognized disease in women worldwide, represents about 30% of all cancers impacting women. This study was aimed to synthesize Cu_2O nanoparticles from the cystoseira myrica algae (CM-Cu_2O NPs) assess their antimicrobial activity against pathogenic bacteria and fungi. We evaluated the expression levels of lncRNAs (*MALAT1* and *GAS5*) and apoptosis genes (*p53, p27, bax, bcl2* and *caspase3*), their prognostic roles.

Methods: In this study, CM-Cu_2O NPs synthesized by cystoseira myrica algae extraction used to evaluate its cytotoxicity and apoptotic properties on MDA-MB-231, SKBR3 and T-47D BC cell lines compared to HDF control cell line. The CM-Cu_2O NPs was characterized by UV–Vis spectroscopy, Fourier transform infrared spectroscopy (FTIR), X-ray diffraction (XRD), Transmission electron microscopy (TEM) and Scanning electron microscopy (SEM). The antimicrobial activity of CM-Cu_2O NPs was assessed against pathogenic bacteria, *staphylococcus aureus* (*S. aureus*) PTCC 1112 bacteria as a standard gram-positive bacteria and *pseudomonas aeruginosa* (*P. aeruginosa*) PTCC 1310 as a standard gram-negative bacterium. Expression profile of *MALAT1* and *GAS5* lncRNAs and apoptosis genes, i.e., *p27, bax, bcl2* and *caspase3* genes, were calculated utilizing qRT-PCR. The changes in the expression levels were determined using the DDCT method.

Results: *MALAT1* was upregulated in MDA-MB-231, SKBR3 and T-47D BC ($p < 0.01$), while *GAS5* was downregulated in SKBR3 and T-47D cell lines tested compared with HDF control cell line ($p < 0.05$) was found. The results revealed that, *p27, bax* and *caspase3* were significantly upregulated in BC cell lines as compared with normal cell line. *Bcl2* expression was also significantly increased in MDA-MB-231 and T47D cell lines compared with normal cell line, but *bcl2* levels were downregulated in SKBR3 cell line.

Conclusions: Our results confirm the beneficial cytotoxic effects of green-synthesized CM-Cu_2O NPs on BC cell lines. This nanoparticle decreased angiogenesis and induces apoptosis, so we conclude that CM-Cu_2O NPs can be used as a supplemental drug in cancer treatments. Significantly, elevated circulating lncRNAs were demonstrated to be BC specific and could differentiate BC cell lines from the normal cell lines. It was demonstrated that lncRNAs used in this study and their expression profiles can be created as biomarkers for early diagnosis and prognosis of BC. Further studies utilizing patients would give recognizable identification of lncRNAs as key players in intercellular interactions.

Keywords: Breast cancer, LncRNA, Cu_2O nanoparticles, Apoptosis genes, Bacteria

Introduction

It is believed that natural compounds obtained from the plant materials are benign and easily metabolized drug in comparison with other synthetic medicinal compounds (Gnanavel et al. 2017). The secondary metabolites obtained from the plant materials have been used to develop drugs (Siegel et al. 2013). Approximately one-fourth of the total medicinal compounds consumed by the developed countries are natural compounds (Rasmussen et al. 2010). At present, the main cancer treatment procedures such as alkylating agents, antimetabolites and other different cancer therapy methods have several side effects because of the incapability of differentiating the normal cell and cancer causing cells that results in toxicity (Ahmad et al. 2013). It is believed that using nanomaterials to treat cancer is a significant procedure to discover the modern cancer drugs (Vinardell and Mitjans 2015). It has been reported that nanoparticles are useful structured modern medicines for treating cancer due to their nanoscale sized feature that results in increased drug effectiveness and sustained release of drug material (Kumar et al. 2012). The brown alga Cystoseira myrica is one of the leading species of brown macroalgae in the Persian Gulf that could be collected economically (Naddafi and Saeedi 2009). Many studies have been done to characterize the metal binding features of many kinds of biomass, but no study has been conducted on brown macro alga Cystoseira myrica until now.

The Cu_2O NPs have distinctive features in the field of nanoscale technological aspect (Gnanavel et al. 2017). The Cu_2O NPs have narrow band gap of 1.7 eV that develops their application in the field of superconductors (Bednorz and Müller 1986; Malandrino et al. 1997), solar energy transformation, synthesis of organic and inorganic nanostructure composites (Vijay Kumar et al. 2001), gas sensors (Ishihara et al. 1998), magnetic resistant equipment's (Zheng et al. 2000), antifungal, antimicrobial, anti-biotic agents (Borkow et al. 2009). The Cu_2O NPs are also applied in pesticide research due to their biocidal features (Borkow and Gabbay 2012) and antibacterial agent (Kumar et al. 2015). It is possible to achieve Cu_2O NPs by microwave irradiations (Wang et al. 2002), sol–gel method (Zhang et al. 2001), electrochemical technique (Yin et al. 2001), thermal decomposition (Gnanavel et al. 2017) and alkoxide supported method (Carnes et al. 2002). These methods have numerous disadvantages chiefly due to the usage of harmful chemicals, high energy utilization and problems to purify the nanoparticles (Ghidan et al. 2016). The process of toxic free green materials like plant extract and microorganisms (Parashar et al. 2009) to prepare nanoparticles would be advantageous for applications in pharmaceutical and drug discovery safety due to toxic free chemicals technique to prepare the nanoparticles (Kumar et al. 2013).

BC in women ranks among the most common malignant tumors; it is also second chief reason of mortality in industrialized countries (Arshi et al. 2018). In 2008, the American Cancer Society estimated that in 2014, roughly 182,500 women would be diagnosed with

BC and 40,500 women would die because of BC (Ye et al. 2010). In Iran, the average age of diagnosis of BC is roughly 15 years lower than the reported cases in western countries (Mousavi et al. 2009). Given the increased number of cancer incidence (Asadzadeh Vostakolaei et al. 2013) and many cancer cases among young individuals in Iran, it is crucial to shed light on disease features and clinical outcomes to help health policy makers in terms of resource allocation, diagnosis, and treatment facilities (Vostakolaei et al. 2012). The etiology of BC is complex and multifactorial. It is believed that genetic, environmental, and reproductive factors are all involved in development of BC (Sapkota et al. 2013). The complex link between circadian rhythm (CR) disruption and BC development could be used as an instance of this etiologic complexity. It has been reported that there is a correlation between disruption in CR and the risk of BC development (Lie et al. 2011). Moreover, it has been shown that there is a link between several epigenetic changes and genomic polymorphisms in genes controlling and BC development (Erdem et al. 2017a; Zienolddiny et al. 2013). Besides, some studies argued that there a correlation between CR disruption and reduced telomere length in which short telomere length itself is linked with BC development (Erdem et al. 2017b).

Apoptosis is a form of programmed cell death signifying a serious tumor-suppressive mechanism activated in response to stress signals like DNA damage, growth factor deprivation, or endoplasmic reticulum (ER) stress (Thandapani and Aifantis 2017). The *p53*, which is believed to be a tumor suppressor, is mutated in about 50% of tumors, often through missense mutations happening in the DNA-binding domain. Apart from influencing the transcriptional activity of *p53*, these missense mutations are frequently linked with an increase in the half-life of *p53* mutant *p53* to accumulate in the tumor cells and often acquire a gain-of-function phenotype. The mutant *p53* is not naturally stable, but some stressors influence the oncogenic activation and features of this protein. For instance, DNA damage and oncogene activation such as RAS mutations, c-myc, or $p16^{INK4a}$ are capable of changing the oncogenic features of mutant *p53* (Dibra et al. 2016). B-cell lymphoma-2 (Bcl-2) family proteins are the main architects in regulating the apoptotic threshold and are often deregulated in cancers (Delbridge and Strasser 2015). The 'BCL-2-regulated' or 'intrinsic' apoptotic pathway integrates stress and survival signaling to determine if a cancer cell will live or die. Actually, several pro-apoptotic members of the BCL-2 family have demonstrated tumor-suppression activity in mouse models of cancer and are lost or repressed in certain human cancers (Delbridge and Strasser 2015). A candidate gene to boost the sensitivity of tumors to conventional treatment is the proapoptotic gene *Bax* (*BCL2* Associated X, Apoptosis Regulator)(Arafat et al. 2000). *Bax* is a protein of the Bcl-2 family promoting apoptosis (Oltval et al. 1993). Studies show that *p53*-mediated cell death is influenced partly through downstream interactions with *Bax* (Xiang et al. 1998). It has also been shown that *Bax* acts as a tumor suppressor gene (Yin et al. 1997). Moreover, mutations of *Bax* have been detected in several human tumors such as those derived from the breast, colon, and ovary (Arafat et al. 2000). Moreover, it has been shown that restoring wild-type *Bax* sensitizes tumor cells to apoptosis (Brimmell et al. 1998; Sakakura et al. 1996). Caspase 3 is the most extensively investigated of the effector caspases. It is involved significantly in both the death receptor pathway, initiated by caspase 8, and the mitochondrial pathway, involving caspase 9. Moreover, several studies reported that caspase 3 activation is obligatory for apoptosis induction in response to chemotherapeutic drugs, e.g., taxanes, 5-fluorouracil, and doxorubicin (O'Donovan et al. 2003). Caspase 3 is produced as an inactive 32-kDa proenzyme, which is cleaved at an aspartate residue to yield a 12-kDa and a 17-kDa subunit. Two 12-kDa and two 17-kDa subunits combine for the formation of the active caspase 3 enzyme. Caspase 3 cleaves various cellular substrates such as structural proteins (e.g., lamins) and DNA repair enzymes [e.g., poly (ADP-ribose) polymerase]. It also activates an endonuclease caspase-activated DNAse that causes the DNA fragmentation that is a feature of apoptosis (Stennicke and Salvesen 1998). *P27* was first introduced as a cell cycle inhibitor in the cells arrested by transforming growth factor β, and the expression of *p27* is regulated by growth inhibitory cytokines and contact inhibition (Matsunobu et al. 2004). *P27* is one of cyclin-dependent kinase inhibitors inhibiting cyclin-dependent kinase activities causing cell cycle arrest. It has been reported that there an inverse correlation between a low level of *p27* expression with the tumor progression or the poor prognosis in several human malignancies including breast, prostate, colon, and lung cancers (Matsunobu et al. 2004; Porter et al. 1997). A recent study using *p27* knockout mice reported that *p27* is involved significantly in inhibiting tumor development and showed the features of a tumor suppressor gene (Nakayama et al. 1996). Overexpression of *p27* by replication-deficient recombinant adenovirus led to apoptosis and reduced malignancy potential in human breast, lung, and prostate cancer cell lines (Katner et al. 2002). Since EWS-Fli1 caused the down-regulation of *p27* in vitro (Matsumoto et al. 2001), *p27* expression could be clinically correlated with disease phenotype, therapeutic responsiveness, and patient result.

Long non-coding RNAs (lncRNAs) are a category of non-coding RNAs, generally longer than 200 bp transcribed from the genome with several regulatory or unknown functions. It has been shown that lncRNAs are obligatory in normal cell and tissue development and differentiation as well as in the initiation and progression of various pathogenic conditions, including cancer (Hrdlickova et al. 2014). In this regard, dysregulated expression of lncRNAs has been reported in BC as well as in several other malignancies (Van Grembergen et al. 2016). Shedding light on the molecular biology of cancer, including that related to the function and behavior of lncRNAs, can help in early detecting as well as in designing targeted therapy for this multifaceted disorder (Hrdlickova et al. 2014). Growth arrest-specific 5 (*GAS5*) is an lncRNA 650 bases in length expressed at high levels during growth arrest. This lncRNA was originally isolated from NIH 3T3 cell line using subtraction hybridization in 1998 (Schneider et al. 1988). The human *GAS5* has been classified as a member of the 59-terminal oligopyrimidine tract (59 TOP) gene family, and this gene is also the host of multiple small nucleolar RNAs within its 11 introns (Smith and Steitz 2015). At least four splice variants have so far been distinguished for *GAS5*, (Raho et al. 2000); it has been reported that this gene is capable of modulating cellular response to numerous apoptotic stimuli such as those prompted by various chemotherapeutic drugs, a concept recommending a mechanism connecting dysregulated *GAS5* expression in cancer with prognosis (Nishimoto et al. 2013). *MALAT1 (Metastasis Associated Lung Adenocarcinoma Transcript 1)* is a highly conserved lncRNA that was first recognized as an upregulated lncRNA in lung cancer with a high tendency to metastasize (Ji et al. 2003). *MALAT1* transcript is found in large quantities in mammalian cells, and the primary transcript is processed into two smaller

RNAs: a long 6.7-kb transcript that localizes to the nuclear speckles (Bernard et al. 2010) and a tRNA-like small RNA (61 nt) that localizes to the cytoplasm (Wilusz et al. 2008). *MALAT1* plays a role in regulating pre-mRNA alternative splicing, and its knockdown leads to cell-cycle arrest (Tripathi et al. 2010). *MALAT1* is also essential for E2F target gene activation by repositioning E2F from polycomb bodies to transcriptionally active nuclear sites in a serum-dependent manner (Yang et al. 2011). Recently, two genome-wide association studies have reported that *MALAT1*, along with NEAT1, binds to the transcription start sites (TSSs) and to the gene bodies of those genes that are actively transcribed (West et al. 2014). It is believed that the overexpression of *MALAT1* is linked to poor prognosis and shorter survival time in early-stage lung cancer (Wang et al. 2017).

We investigated the effect of CM-Cu_2O NPs on MDA-MB-231, SKBR3 and T-47D BC cell lines. Furthermore, we hypothesized that expression signatures of the profile of two lncRNAs (*MALAT1* and *GAS5*) and four apoptosis genes (*p53*, *p27*, *bax*, *bcl2* and *caspase3*) may be useful biomarkers for diagnosis, prognosis, or prediction of BC. The expression levels were evaluated by qRT-PCR.

Materials and methods

Materials

The brown macroalga was gathered from the Persian Gulf on the coast of Bandar Bushehr, Iran (28° 58′ N 50° 50′ E). Sigma Aldrich Chemicals (Ltd., Mumbai, India) provided the study with copper chloride ($CuCl_2$) and ethanol.

Preparing Cystoseira myrica leaf extract

The Cystoseira myrica were washed in running tap water for removing the filth and dust. The biomass was put to dry in the shade in a room temperature for about 72 h. By applying a mechanical grinder, the dried leaves materials were made into fine particles. Ethanol was applied by Soxhlet apparatus to extract the plant material for 4 h, which were subjected to rotary evaporator for removing the extra solvent. The concentrated ethanolic leaves extract of Cystoseira myrica were filtered and gathered for further process.

Preparing Cu_2O nanoparticles

Approximately 50 ml of freshly prepared 0.003 M hydrated $CuCl_2$ solution was mixed with 50 ml of ethanolic leaves extract of Cystoseira myrica and boiled for 3 h at 60 °C accompanied with incessant stirring. UV–visible spectroscopy was applied to monitor Cu_2O NPs formations. Because of the surface plasmon resonance excitation, the color turned from yellow to brown showing the formation of Cu_2O NPs. After observing the color change, the prepared content was put for centrifuging at 3000 rpm for 20 min. Distilled water was used to wash the formed pellets, which were kept in using crucible at 400 °C for 2 h.

Characterizing Cu_2O nanoparticles

Several analytical techniques like UV–visible Spectroscopy (Shimadzu UV-1800 PC, Japan) between the wavelength of 200–800 nm 62 were applied to confirm the formation of CM-Cu_2O NPs (Roopan et al. 2014). Advance Power XRD, model D8 (Bruker, Germany) was used to perform the X-Ray Diffractometer (XRD) analysis for the synthesized

Cu_2O NPs. The Scherrer formula was applied for calculating the particle size determination using the formula, $D = K\lambda/\beta \mathrm{Cos}\theta$, where D shows the particle size, λ shows the wavelength, K denotes a Scherrer constant having value of 0.94, β is a half width maximum and θ shows the diffraction angle. FT-IR Spectroscopy (Bruker, Germany) was applied between the wave number of 400 $cm^{-1}$to 4000 cm^{-1} to detect the functional group present in the synthesized Cu_2O NPs. Transmission electron microscopy (TEM) and Scanning Electron Microscope (SEM) were applied to determine the shape of the synthesized Cu_2O NPs.

Preparing microbial isolates

Tested organisms were common human pathogens, some of which are antibiotic resistant, involving staphylococcus aureus (*S. aureus*) PTCC 1112 bacteria as a standard gram-positive bacteria and *Pseudomonas aeruginosa* (*P. aeruginosa*) PTCC 1310 as a standard gram-negative bacterium obtained from the Iranian Research Organization for Science and Technology, Tehran, Iran. Isolates were kept fresh on nutrient agar plates (Oxoid) and on nutrient broth (Oxoid) with 15% glycerol and kept at −4 °C for future use. Small inoculum of each of the pure, fresh cultures was added to 5 ml sterile distilled water making a 0.5 Mac Farland bacterial suspension, which was put for inoculation on Muller Hinton agar plate surfaces.

Antimicrobial assay

The agar well diffusion technique was applied for the antimicrobial activity in vitro (Vanden Berghe et al. 1991). A sterile cotton swab was used to spread the small inoculum of each of the prepared bacterial evenly onto Muller Hinton agar plate surfaces (Oxoid). Before inoculation, plates were put to rest at room temperature for the absorption of the microbial inoculums. A 5–7 mm diameter sterile cork borer was applied to make 4 equidistant wells on each MH plates corresponding to the dry and fresh *S. aureus* and *P. aeruginosa*. 100ll of the appropriate seaweed extracts was used to load the wells. Before inoculation, plates were put to rest at room temperature for 30 min for enhanced absorption; then, plates were put for incubation at 37 °C for 18–24 h. All tests were performed in duplicate. The inhibition zone around each well was determined to show the antimicrobial activity. Mean diameter values were determined from duplicate runs of each assay. The effectiveness of the target algal extracts was compared with standard antibiotic disks, methanol and acetone used as positive and negative controls, in the respective order.

Cell culture

The Institute of the Chinese Academy of Sciences (Shanghai, China) provided the study with the MDA-MB-231 (ATCC HTB-26), SKBR3 (ATCC HTB-30), T-47D (ATCC HTB-133) and HDF (ATCC PCS-201-012) cell lines. The MDA-MB-231, SKBR3 and T-47D cell lines were cultured and kept in RPMI-1640 medium (Sigma-Aldrich, St. Louis, MO, USA) supplemented with L-Glutamine (Sigma-Aldrich, St. Louis, MO, USA), 10% fetal bovine serum (Gibco, Carlsbad, CA, USA), 100 U/ml penicillin (Sigma-Aldrich, St. Louis, MO, USA), and 100 µg/ml streptomycin (Sigma-Aldrich, St. Louis, MO, USA) in a cell culture incubator at 37 °C, 5% CO_2, and 95% humidity. HDF cells were used as non-cancer cell group during the experiment (control cell).

Cell take-up and Cu's delivery into cell medium

The cell take-up of nanoparticles and Cu delivery to the medium were dictated by inductively coupled plasma-mass spectrometry (ICP-MS) (Thermo Elemental X series 2, USA). For that, the exposed cells were harvested and counted, then cells were processed by treatment with nitric corrosive for 8 h in 37 °C (Abudayyak et al. 2020).

MTT assay

The viable MDA-MB-231 (ATCC HTB-26), SKBR3 (ATCC HTB-30), T-47D (ATCC HTB-133) and HDF (ATCC PCS-201-012) cell lines with a concentration of 5×103 (100 μl/well) were cultured in flat bottom 96-well plates for 24 h for performing the MTT assay; then, the supernatant was replaced by 100 μl RPMI medium containing CM-Cu_2O NPs (0, 5, 10, 15, 30, 45, 60, 75, 90 and 120 μg/ml). Experiments are performed in triplicate for each incubation time (24, 48, and 72 h). After the end of the incubations, the MTT solution, at the final concentration of 4 mg/ml in PBS, was added to each well and incubation was done for 4 h at 37 °C in a 5% CO_2 atmosphere; Next, the supernatant was once more replaced by DMSO (100 μl). After the end of assay, shaking was applied for 10 min and the plate was read against a blank reagent at 570 nm. The cytotoxicity of samples on cells was expressed as IC50 that is a concentration of the tested samples and reduces 50% of cellular growth than untreated control sample and was determined using the following formula:

$$\text{Growth inhibition} = \text{OD control} - \text{OD treated sample} \times 100/\text{OD control}.$$

Flow cytometry-based cell cycle assay

PI staining was performed for the cell cycle analysis followed by flow cytometry. Briefly, HDF, MDA-MB-231, SKBR3 and T-47D cells were treated with slightly different concentrations of nanoparticles (0, 5, 10, 15, 30, 45, 60, 75, 90 and 120 μg/ml). Treated and untreated control cells were harvested, washed double with phosphate-buffered saline (PBS), and glued in cold grain alcohol (70%) for four h at 4 °C. The mounted cells were washed, pelleted, resuspended in PBS, stained with an answer containing PI and RNase (40 μg/ml and 100 μg/ml, respectively) and incubated at 37 °C for thirty min until analysis. Flow cytometry was performed victimization associate Epics Altra flow cytometer (Beckman Coulter) at associate excitation wavelength of 488 nm and an emission wavelength of 610 nm. The information collected for 2×104 cells per condition were analyzed using WinMDI 2.8 software.

RNA Extraction and cDNA Synthesis

The RNX-Plus solution (SinaClon, Iran) was applied according to the manufacturer's instructions to extract total RNA from cells. Thermo Scientific NanoDrop 2000 Spectrophotometer (Thermo Scientific, Germany) was applied to determine the purity and concentration of the extracted RNA; gel electrophoresis was done to verify the integrity of the RNA. After extracting RNA, a *DNase*I treatment (EN0521, Fermentas, Germany) was carried out; 1 µg RNA was then applied for cDNA synthesis through the application of random hexamers as primers and Prime Script-RT kit (Takara, Japan).

Real-time qPCR

Specific primers (Table 1) and SYBR Premix Ex Taq II kit (Takara, Japan) were applied according to the manufacturer's instruction for real-time qPCR. Rotor gene 6000 Corbett detection system was used for amplification. The thermal cycling condition was set as follows: an initial activation step for 5 min at 95 °C, followed by 40 cycles of 95 °C for 15 s and 65 °C for 1 min. No template controls (NTCs) were also applied in each run. A series of experiments was done with varying primer combinations (Table 1) to detect the best primer concentrations. Standard curves were prepared for each primer set using data from serially diluted samples for confirming the reaction efficacies. Melting curve analyses were also done for each primer set. Moreover, PCR products were electrophoresed on 2% agarose gel for confirming the product sizes. The *GAPDH* housekeeping gene was applied as a normalizer, and the HDF cell line as the control group for the cancer cell lines. Relative expressions were determined by applying the $2-\Delta\Delta CT$ method. The qPCR assays were performed in triplicate, and the data are presented as the mean ± SEM where applicable.

Statistical analysis

GraphPad Prism 7.00 (GraphPad, La Jolla, CA, USA) was applied to analyze Data and statistical tests. Unpaired t-Test was used to compare the survival rates between treat group and the untreat group (control). Means were compared using a one-way analysis of variance (ANOVA), followed by a Tukey–Kramer post hoc test using a 95% confidence interval. Differences were considered significant at $p < 0.05$.

Table 1 Sequences and optimized concentration of primers used in this study

Primers	Primer Sequences (5′ to 3′)	Primer concentrations (nM)	Annealing temperature (°C)	Product size (bp)
GAPDH	AATGGGCAGCCGTTAGGAAA	300	55	168
	GCGCCCAATACGACCAAATC	300		
p27	TGGAGAAGCACTGCAGAGAC	300	53	252
	GCGTGTCCTCAGAGTTAGCC	600		
p53	TACTCCCCTGCCCTCAACAAGA	300	55	181
	CGCTATCTGAGCAGCGCTCATG	300		
bax	TCTGACGGCAACTTCAACTG	600	56	188
	TTGAGGAGTCTCACCCAACC	900		
Bcl2	GGATGCCTTTGTGGAACTGT	300	63	236
	AGCCTGCAGCTTTGTTTCAT	600		
Caspase 3	CGGGGTACGGAGCTGGACTGT	300	58	251
	AATTCCGTTGCCACCTTCCTGTT	300		
GAS5	TGAAGTCCTAAAGAGCAAGCC	900	52	120
	ACCAGGAGCAGAACCATTAAG	300		
MALAT1	ATGCGAGTTGTTCTCCGTCT	300	52	118
	TATCTGCGGTTTCCTCAAGC	300		

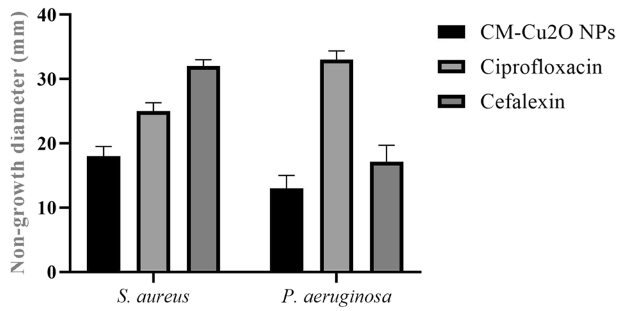

Fig. 1 Data for the Growth diameter (mm) after 72 h of incubation at temperature range of 15–30 °C

Table 2 IC50 values of HDF, MDA, SKBR and T47D cells lines incubated with CM-Cu_2O NPs for 24, 48 and 72 h

IC50	IC50 values (µg/ml)		
	24 h	**48 h**	**72 h**
HDF	207.64	208.85	227.53
MDA	29.95	29.99	30.03
SKBR	22.18	24.65	24.40
T47D	26.93	23.84	20.46

Results

Antimicrobial assay of CM-Cu_2O NPs

Figure 1 shows the in vitro antimicrobial activity of the dried seaweeds; CM-Cu_2O NPs, ciprofloxacin and cefalexin. Among the dried extracts, *S. aureus* and *P. aeruginosa* was the most effective displaying the largest inhibition zone especially with CM-Cu_2O NPs. Moreover, CM-Cu_2O NPs exhibited variable antibacterial influence against some isolates, but higher in comparison with the standard antibiotic disks being used (Table 2).

UV–visible spectral analysis of CM-Cu_2O NPs

The UV spectral analysis for the synthesized CM-Cu_2O NPs were done at regular interval of time. The color change from yellow to brown color primarily indicates the conversion of Cu into Cu_2O NPs. The UV spectrum of the synthesized CM-Cu_2O NPs evidently indicates the progression and stability, as shown in Fig. 2. The surface plasmon resonances of the CM-Cu_2O NPs were confirmed by the appearance of maximum absorbance at the 200 nm.

FT-IR analysis of CM-Cu_2O NPs

The FT-IR transmittance analysis was done for determining the functional groups present in the synthesized CM-Cu_2O NPs. The FT-IR analysis shows different characteristics peaks at 612.06 cm^{-1}, 1217.15 cm^{-1}, 1738.57 cm^{-1} and 3016.89 cm^{-1} between the range 600–4000 cm^{-1} (Fig. 3). The slight broad band at 3016.89 cm^{-1} corresponds to the N–H stretch due to amine group and the peak at 1738.57 cm^{-1}

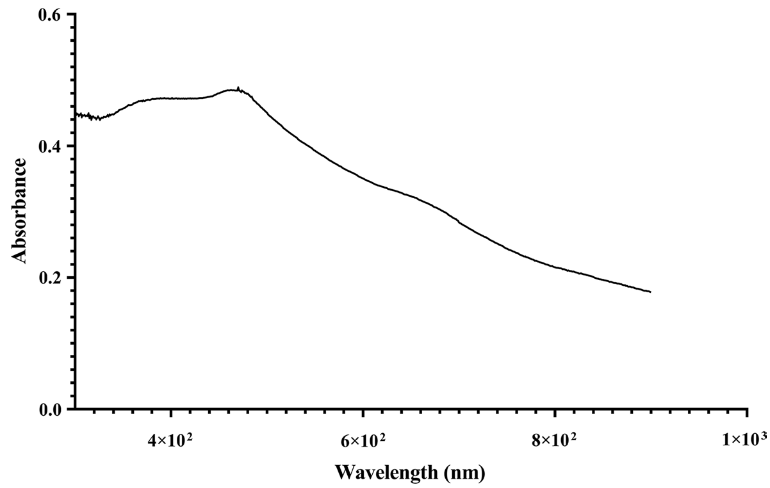

Fig. 2 UV–Visible spectrum of the synthesized CM-Cu_2O NPs

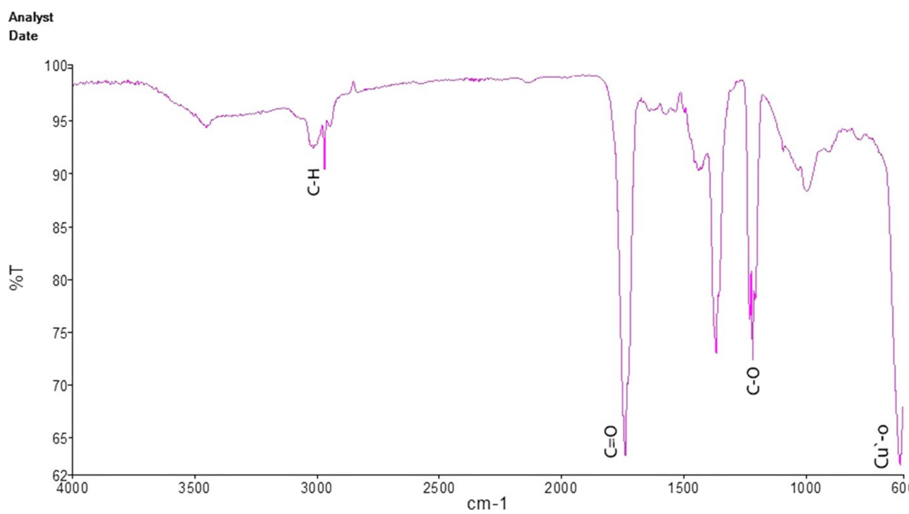

Fig. 3 FTIR spectrum of the synthesized CM-Cu_2O NPs

shows the presence C=O bending due to the presence of aromatic secondary metabolites. The band at 1738.57 cm^{-1} shows the presence of C–O bending due to the alkene group. The prominent peak at 612.06 cm^{-1} confirms the presence the Cu–O vibration in the synthesized CuO NPs (Davoodi et al. 2013).

XRD, TEM and SEM analysis of CM-Cu_2O NPs

The X-ray diffractometer (XRD) analyses were carried out for the synthesized CM-Cu_2O NPs for verifying the crystalline nature of synthesized nanoparticles (Fig. 4). The XRD analysis of the Cu_2O NPs was interconnected with the Joint Committee on Powder Diffraction Standards (JCPDS) verifying the crystalline nature of Cu_2O NPs (JCPDS 96-901-5925). TEM (Fig. 5-A) and SEM (Fig. 5-B) were done to ascertain the morphological studies for the synthesized CM mediated Cu_2O NPs. The SEM analysis

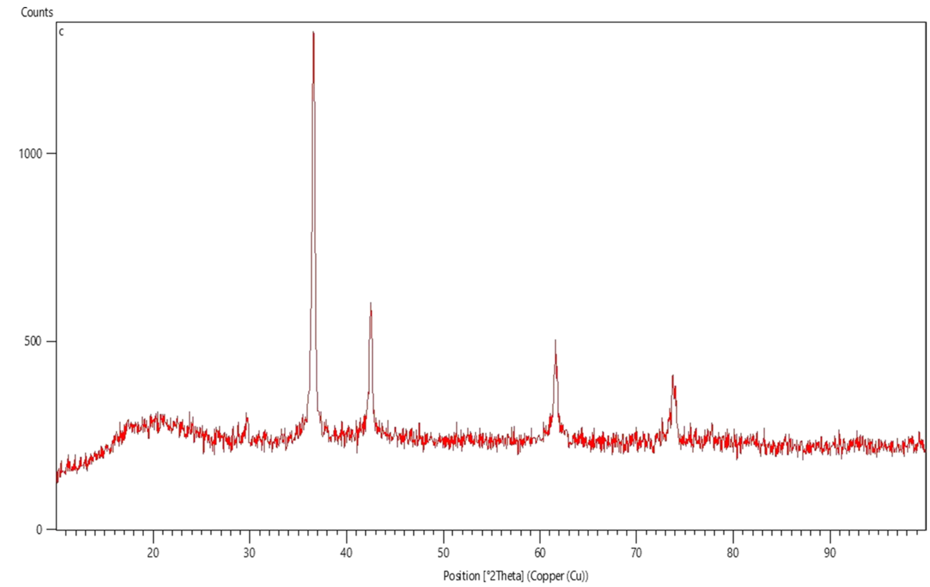

Fig. 4 XRD pattern of synthesized CM-Cu_2O NPs

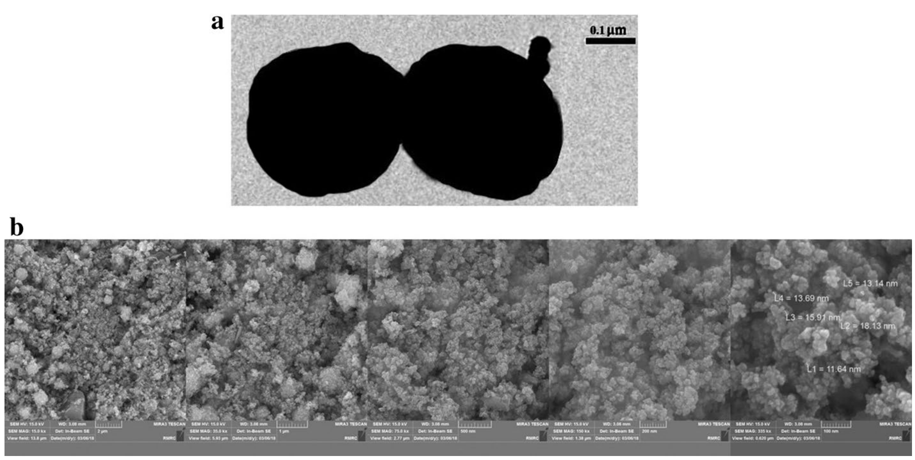

Fig. 5 TEM (**a**) and SEM (**b**) images of synthesized CM-Cu_2O NPs

for the synthesized nanoparticles showed the formation of CM-Cu_2O NPs around 2 µm, 1 µm, 500 nm, 200 nm and 100 nm in an agglomerated cluster forms as shown in the (Fig. 5-B).

Cell take-up and Cu's delivery into cell medium

The ICP-MS test results demonstrate that Cu particles were not distinguished in cell-free medium, while approximately 4% of the exposure dose was detected in the cells, which indicates the uptake of Cu_2O-NPs by HDF, MDA-MB-231, SKBR3 and T-47D cell lines following exposure for 24 h (Table 3). Cu_2 substance of the unexposed cell (NC) was additionally estimated for each cell line.

Table 3 Assessment of the cellular uptakes of CuO-NPs

Cells	Exposure concentration (μg/ml/10^5 cells)	Cu amount (ng/10^5 cells)
HDF	Negative control	129 ± 1.1
	15	286 ± 5.3
	30	495 ± 2.3
MDA-MB-231	Negative control	132 ± 2.5
	15	315 ± 1.6
	30	312 ± 6.3
SKBR3	Negative control	135 ± 2.3
	15	245 ± 4.3
	30	480 ± 2.2
T-47D	Negative control	136 ± 3.1
	15	302 ± 1.9
	30	522 ± 4.6

CM-Cu_2O NPs-induced inhibition of proliferation

MTT: Cytotoxicity effect of CM-Cu_2O NPs was evaluated on four human cancer cells, i.e., HDF, MDA, SKBR and T47D. All cells were treated with different concentration of CM-Cu_2O NPs for incubation time of 24, 48 and 72 h. MTT was used to measure cell viability. The values of IC50 (μg/ml) were obtained for the cells. As presented in Table 2, the values of IC50 (μg/ml) were decreased in time of incubation dependent manner (Fig. 6a).

PI: Following treatment of cells with different concentrations of CM-Cu_2O NPs, the findings revealed that the proliferation of MDA, SKBR and T47D cells was substantially inhibited at 15 μg/ml; these variations were statistically important compared to the corresponding values in the Cu-NPs (Fig. 6b).

Expression of apoptosis genes in BC cell lines

According to qPCR analysis on RNA samples from cancer cell lines, all of apoptosis genes, i.e., *p53, p27, bax, bcl2* and *caspase3* genes, were overexpressed in MDA-MB-231, SKBR3 and T-47D BC cell lines in comparison with HDF control cell line (Fig. 7).

LncRNA Expression Profiles in BC cell lines

The qRT-PCR was applied to assess the transcriptional status of *MALAT1* and *GAS5* lncRNAs in BC cell lines for incubation time of 24, 48 and 72 h. In comparison with the average expression in normal cell line, *MALAT1* was upregulated in MDA-MB-231, SKBR3 and T-47D BC cell lines and *GAS5* was upregulated in SKBR3 cell line tested (Fig. 8). While *GAS5* exhibited lower expression levels in MDA-MB-231 and T-47D cell lines. While *MALAT1* showed a fairly similar overexpression pattern in 24 h SKBR3 cell line and *GAS5* showed lower expression levels in 72 h cell lines. We found a significant difference for *MALAT1* and *GAS5* lncRNAs ($p < 0.001$).

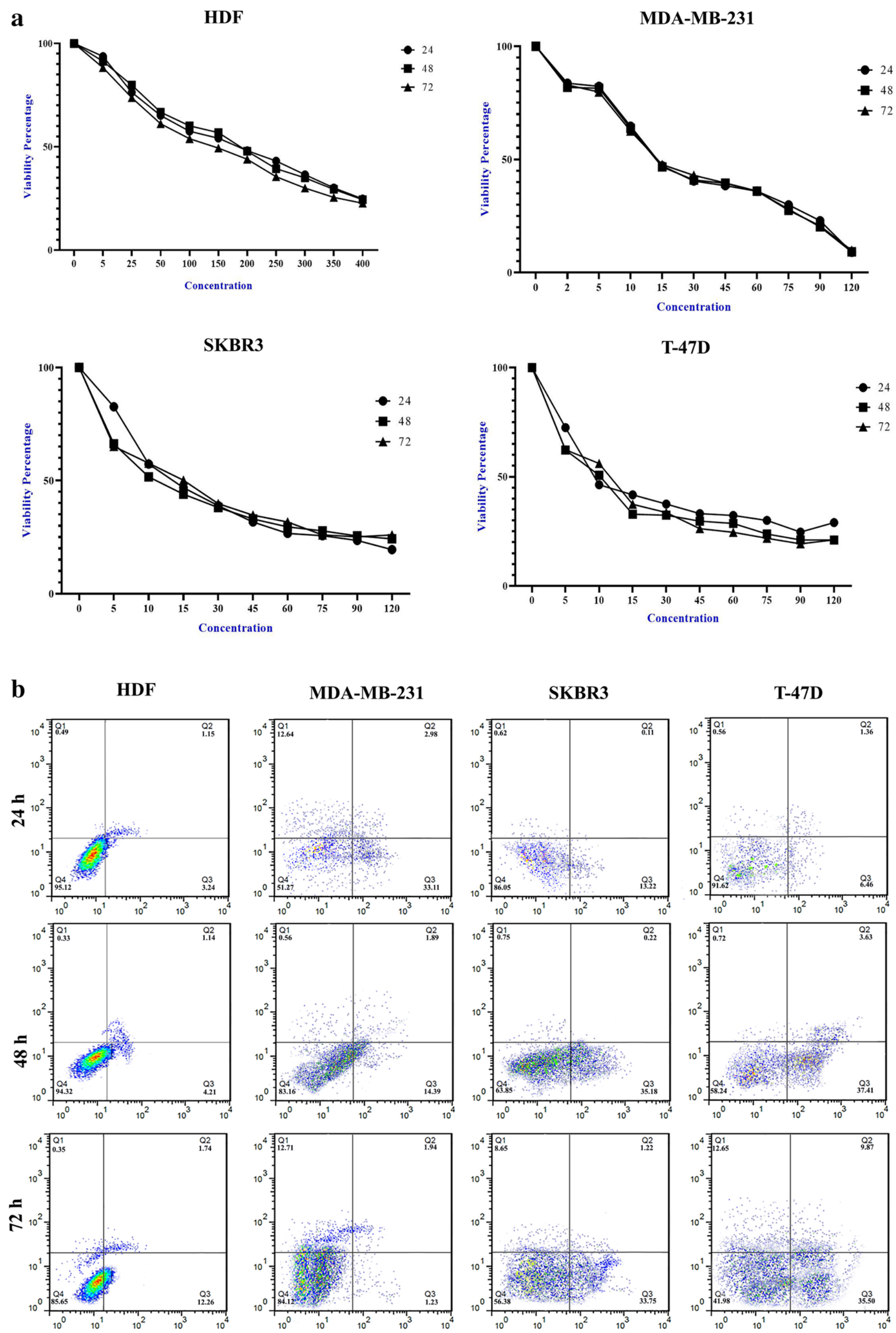

Fig. 6 Cytotoxicity of CM-Cu_2O NPs in HDF, MDA-MB-231, SKBR3 and T-47D cells. **a** CM-Cu_2O NPs decreased growth and proliferation of HDF, MDA, SKBR and T47D cells in concentration-dependent manner in all the time of incubation by MTT method and **b** Flow cytometry assays assess the apoptotic activity of paclitaxel-treated cells in HDF, MDA-MB-231, SKBR3 and T-47D at 24, 48 and 72 h post-treatment

Correlations between the Expression of the lncRNAs

Table 4 shows the correlations between lncRNAs expression. There were no significant correlations between the lncRNAs expression. Error bars show the minimum and maximum variables.

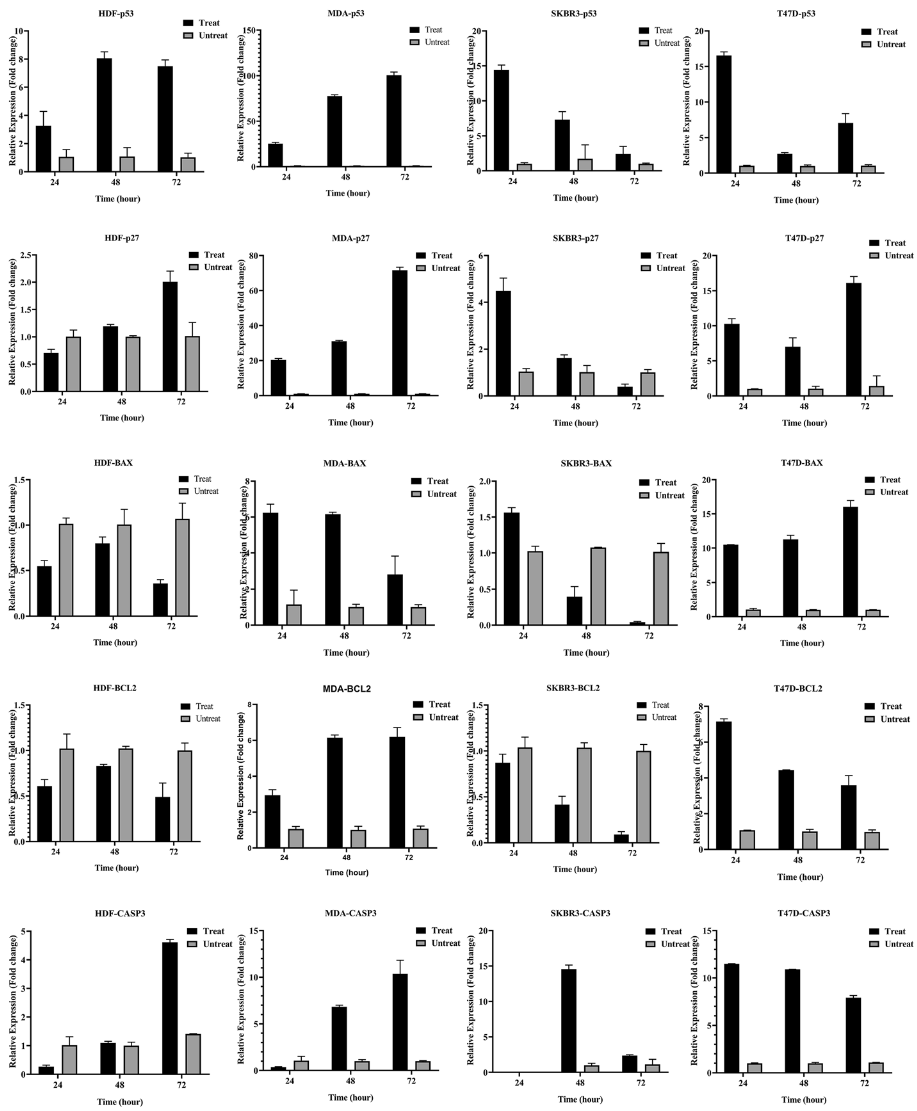

Fig. 7 Expression levels of apoptosis genes, i.e., *p53*, *p27*, *bax*, *bcl2* and *caspase3* genes in BC cell lines for incubation time of 24, 48 and 72 h compared to normal cell line. qRT-PCR was used to quantify the expression levels of *p53*, *p27*, *bax*, *bcl2* and *caspase3* genes in BC cell lines. * Significant at the 0.05 level; **significant at the 0.001 level; ***significant at the 0.0001 level. Error bars show the minimum and maximum variables

Correlations between the expression of the apoptosis genes

Table 5 shows the correlations among apoptosis genes (*p53*, *p27*, *bax*, *bcl2* and *caspase3*). There were significant correlations between the lncRNAs expression ($p > 0.05$).

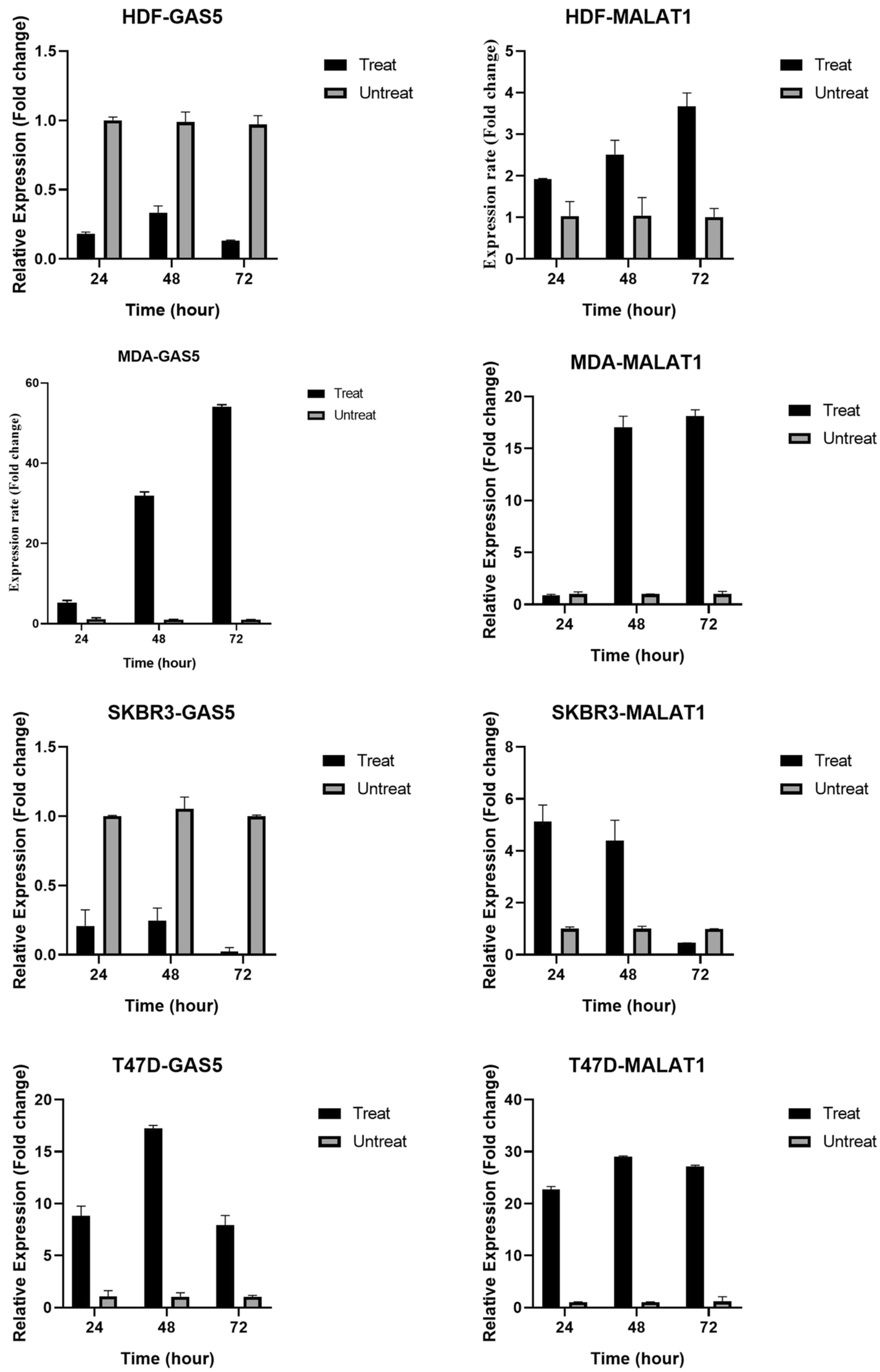

Fig. 8 Expression levels of lncRNAs in BC cell lines for incubation time of 24, 48 and 72 h compared to normal cell lines. qRT-PCR was used to quantify the expression levels of *GAS5* and *MALAT1* lncRNAs in BC cell lines. Error bars show the minimum and maximum variables

Table 4 Correlation between LncRNA Expression

		HDF-GAS5	HDF-*MALAT1*	MDA-GAS5	MDA-*MALAT1*	SKBR3-GAS5	SKBR3-*MALAT1*	T47D-GAS5	T47D-*MALAT1*
HDF-GAS5	Correlation coefficient	1	−0.410	−0.186	0.227	0.794	0.577	0.988	0.545
	Significance (2-tailed)	0	0.730	0.880	0.853	0.415	0.608	0.095	0.632
HDF-*MALAT1*	Correlation coefficient	−0.410	1	0.972	0.794	−0.879	−0.981	−0.268	0.540
	Significance (2-tailed)	0.730	0	0.149	0.415	0.315	0.122	0.826	0.636
MDA-GAS5	Correlation coefficient	−0.186	0.972	1	0.914	−0.744	−0.909	−0.036	0.722
	Significance (2-tailed)	0.880	0.149	0	0.265	0.465	0.272	0.976	0.486
MDA-*MALAT1*	Correlation coefficient	0.227	0.794	0.914	1	−0.410	−0.663	0.371	0.940
	Significance (2-tailed)	0.853	0.415	0.265	0	0.730	0.538	0.757	0.220
SKBR3-GAS5	Correlation coefficient	0.794	−0.879	−0.744	−0.410	1	0.954	0.694	−0.075
	Significance (2-tailed)	0.415	0.315	0.465	0.730	0	0.192	0.511	0.951
SKBR3-*MALAT1*	Correlation coefficient	0.577	−0.981	−0.909	−0.663	0.954	1	0.448	−0.369
	Significance (2-tailed)	0.608	0.122	0.272	0.538	0.192	0	0.704	0.758
T47D-GAS5	Correlation coefficient	0.988	−0.268	−0.036	0.371	0.694	0.448	1	0.664
	Significance (2-tailed)	0.095	0.826	0.976	0.757	0.511	0.704	0	0.537
T47D-*MALAT1*	Correlation coefficient	0.545	0.540	0.722	0.940	−0.075	−0.369	0.664	1
	Significance (2-tailed)	0.632	0.636	0.486	0.220	0.951	0.758	0.537	0

Correlations between lncRNAs expression and apoptosis genes

Table 6 shows the correlations between lncRNAs expression (*MALAT1* and *GAS5*) and apoptosis genes (*p53*, *p27*, *bax*, *bcl2* and *caspase3*). There was a significant correlation between lncRNAs expression and apoptosis genes ($p > 0.05$).

Table 5 Correlation between apoptosis genes

		HDF-p53	HDF-p27	HDF-BAX	HDF-BCL2	HDF-CASP3	MDA-p53	MDA-p27	MDA-BAX	MDA-BCL2	MDA-CASP3	SKBR3-p53	SKBR3-p27	SKBR3-BAX	SKBR3-BCL2	SKBR3-CASP3	T47D-p53	T47D-p27	T47D-BAX	T47D-BCL2	T47D-CASP3
HDF-p53	Correlation coefficient	1.000	0.714	0.194	0.278	0.561	0.917	0.576	−0.421	0.993	0.894	−0.865	−0.919	−0.945	−0.860	0.706	−0.979	0.054	0.516	−0.943	−0.538
	Significance (2-tailed)	0.000	0.494	0.876	0.821	0.621	0.261	0.609	0.723	0.075	0.296	0.335	0.258	0.211	0.341	0.501	0.130	0.966	0.655	0.216	0.638
HDF-p27	Correlation coefficient	0.714	1.000	−0.549	−0.475	0.980	0.933	0.984	−0.936	0.791	0.952	−0.969	−0.932	−0.903	−0.971	0.007	−0.557	0.738	0.968	−0.906	−0.974
	Significance (2-tailed)	0.494	0.000	0.630	0.685	0.127	0.234	0.115	0.229	0.419	0.198	0.159	0.237	0.283	0.153	0.995	0.624	0.472	0.161	0.279	0.144
HDF-BAX	Correlation coefficient	0.194	−0.549	1.000	0.996	−0.703	−0.212	−0.690	0.808	0.077	−0.267	0.325	0.208	0.136	0.334	0.832	−0.389	−0.969	−0.740	0.143	0.723
	Significance (2-tailed)	0.876	0.630	0.000	0.055*	0.503	0.864	0.515	0.401	0.951	0.828	0.789	0.867	0.913	0.783	0.374	0.746	0.159	0.470	0.909	0.486
HDF-BCL2	Correlation coefficient	0.278	−0.475	0.996	1.000	−0.640	−0.128	−0.625	0.755	0.162	−0.183	0.242	0.123	0.051	0.252	0.876	−0.467	−0.944	−0.680	0.057	0.661
	Significance (2-tailed)	0.821	0.685	0.055*	0.000	0.558	0.918	0.570	0.456	0.896	0.883	0.844	0.921	0.968	0.838	0.320	0.691	0.213	0.524	0.963	0.541
HDF-CASP3	Correlation coefficient	0.561	0.980	−0.703	−0.640	1.000	0.844	1.000	−0.987	0.655	0.873	−0.901	−0.841	−0.800	−0.905	−0.191	−0.381	0.857	0.999	−0.804	−1.000
	Significance (2-tailed)	0.621	0.127	0.503	0.558	0.000	0.360	0.012*	0.102	0.546	0.325	0.286	0.363	0.410	0.280	0.878	0.751	0.345	0.034	0.405	0.017*
MDA-p53	Correlation coefficient	0.917	0.933	−0.212	−0.128	0.844	1.000	0.854	−0.747	0.958	0.998	−0.993	−1.000	−0.997	−0.992	0.366	−0.818	0.447	0.814	−0.997	−0.829
	Significance (2-tailed)	0.261	0.234	0.864	0.918	0.360	0.000	0.348	0.463	0.185	0.036*	0.074	0.003**	0.049*	0.081	0.762	0.391	0.705	0.394	0.045	0.378
MDA-p27	Correlation coefficient	0.576	0.984	−0.690	−0.625	1.000	0.854	1.000	−0.984	0.669	0.882	−0.909	−0.851	−0.811	−0.913	−0.172	−0.398	0.847	0.997	−0.815	−0.999
	Significance (2-tailed)	0.609	0.115	0.515	0.570	0.012*	0.348	0.000	0.114	0.534	0.313	0.274	0.351	0.398	0.268	0.890	0.739	0.357	0.046	0.393	0.029*
MDA-BAX	Correlation coefficient	−0.421	−0.936	0.808	0.755	−0.987	−0.747	−0.984	1.000	−0.525	−0.784	0.820	0.744	0.694	0.825	0.345	0.228	−0.928	−0.994	0.698	0.991
	Significance (2-tailed)	0.723	0.229	0.401	0.456	0.102	0.463	0.114	0.000	0.648	0.427	0.388	0.466	0.512	0.382	0.776	0.853	0.243	0.069	0.508	0.085

Table 5 (continued)

		HDF-p53	HDF-p27	HDF-BAX	HDF-BCL2	HDF-CASP3	MDA-p53	MDA-p27	MDA-BAX	MDA-BCL2	MDA-CASP3	SKBR3-p53	SKBR3-p27	SKBR3-BAX	SKBR3-BCL2	SKBR3-CASP3	T47D-p53	T47D-p27	T47D-BAX	T47D-BCL2	T47D-CASP3
MDA-BCL2	Correlation coefficient	0.993	0.791	0.077	0.162	0.655	0.958	0.669	−0.525	1.000	0.940	−0.918	−0.959	−0.977	−0.914	0.617	−0.948	0.171	0.614	−0.976	−0.634
	Significance (2-tailed)	0.075	0.419	0.951	0.896	0.546	0.185	0.534	0.648	0.000	0.221	0.260	0.182	0.136	0.266	0.576	0.205	0.890	0.579	0.140	0.563
MDA-CASP3	Correlation coefficient	0.894	0.952	−0.267	−0.183	0.873	0.998	0.882	−0.784	0.940	1.000	−0.998	−0.998	−0.991	−0.998	0.313	−0.784	0.496	0.846	−0.992	−0.859
	Significance (2-tailed)	0.296	0.198	0.828	0.883	0.325	0.036	0.313	0.427	0.221	0.000	0.038	0.039	0.085	0.045	0.798	0.427	0.669	0.358	0.081	0.342
SKBR3-p53	Correlation coefficient	−0.865	−0.969	0.325	0.242	−0.901	−0.993	−0.909	0.820	−0.918	−0.998	1.000	0.993	0.981	1.000	−0.255	0.745	−0.548	−0.876	0.982	0.888
	Significance (2-tailed)	0.335	0.159	0.789	0.844	0.286	0.074	0.274	0.388	0.260	0.038*	0.000	0.077	0.124	0.006**	0.836	0.465	0.631	0.320	0.119	0.304
SKBR3-p27	Correlation coefficient	−0.919	−0.932	0.208	0.123	−0.841	−1.000	−0.851	0.744	−0.959	−0.998	0.993	1.000	0.997	0.991	−0.370	0.820	−0.442	−0.812	0.998	0.826
	Significance (2-tailed)	0.258	0.237	0.867	0.921	0.363	0.003**	0.351	0.466	0.182	0.039*	0.077	0.000	0.046*	0.084	0.759	0.388	0.708	0.397	0.042*	0.381
SKBR3-BAX	Correlation coefficient	−0.945	−0.903	0.136	0.051	−0.800	−0.997	−0.811	0.694	−0.977	−0.991	0.981	0.997	1.000	0.979	−0.437	0.860	−0.376	−0.767	1.000	0.783
	Significance (2-tailed)	0.211	0.283	0.913	0.968	0.410	0.049*	0.398	0.512	0.136	0.085	0.124	0.046*	0.000	0.130	0.712	0.341	0.754	0.443	0.004**	0.427
SKBR3-BCL2	Correlation coefficient	−0.860	−0.971	0.334	0.252	−0.905	−0.992	−0.913	0.825	−0.914	−0.998	1.000	0.991	0.979	1.000	−0.245	0.738	−0.556	−0.881	0.981	0.893
	Significance (2-tailed)	0.341	0.153	0.783	0.838	0.280	0.081	0.268	0.382	0.266	0.045*	0.006	0.084	0.130	0.000	0.843	0.471	0.624	0.313	0.126	0.297
SKBR3-CASP3	Correlation coefficient	0.706	0.007	0.832	0.876	−0.191	0.366	−0.172	0.345	0.617	0.313	−0.255	−0.370	−0.437	−0.245	1.000	−0.835	−0.669	−0.242	−0.430	0.217
	Significance (2-tailed)	0.501	0.995	0.374	0.320	0.878	0.762	0.890	0.776	0.576	0.798	0.836	0.759	0.712	0.843	0.000	0.371	0.533	0.844	0.717	0.860
T47D-p53	Correlation coefficient	−0.979	−0.557	−0.389	−0.467	−0.381	−0.818	−0.398	0.228	−0.948	−0.784	0.745	0.820	0.860	0.738	−0.835	1.000	0.150	−0.332	0.856	0.356
	Significance (2-tailed)	0.130	0.624	0.746	0.691	0.751	0.391	0.739	0.853	0.205	0.427	0.465	0.388	0.341	0.471	0.371	0.000	0.904	0.785	0.346	0.769

Table 5 (continued)

		HDF-p53	HDF-p27	HDF-BAX	HDF-BCL2	HDF-CASP3	MDA-p53	MDA-p27	MDA-BAX	MDA-BCL2	MDA-CASP3	SKBR3-p53	SKBR3-p27	SKBR3-BAX	SKBR3-BCL2	SKBR3-CASP3	T47D-p53	T47D-p27	T47D-BAX	T47D-BCL2	T47D-CASP3
T47D-p27	Correlation coefficient	0.054	0.738	−0.969	−0.944	0.857	0.447	0.847	−0.928	0.171	0.496	−0.548	−0.442	−0.376	−0.556	−0.669	0.150	1.000	0.883	−0.382	−0.871
	Significance (2-tailed)	0.966	0.472	0.159	0.213	0.345	0.705	0.357	0.243	0.890	0.669	0.631	0.708	0.754	0.624	0.533	0.904	0.000	0.311	0.750	0.327
T47D-BAX	Correlation coefficient	0.516	0.968	−0.740	−0.680	0.999	0.814	0.997	−0.994	0.614	0.846	−0.876	−0.812	−0.767	−0.881	−0.242	−0.332	0.883	1.000	−0.771	−1.000
	Significance (2-tailed)	0.655	0.161	0.470	0.524	0.034	0.394	0.046	0.069	0.579	0.358	0.320	0.397	0.443	0.313	0.844	0.785	0.311	0.000	0.439	0.016*
T47D-BCL2	Correlation coefficient	−0.943	−0.906	0.143	0.057	−0.804	−0.997	−0.815	0.698	−0.976	−0.992	0.982	0.998	1.000	0.981	−0.430	0.856	−0.382	−0.771	1.000	0.787
	Significance (2-tailed)	0.216	0.279	0.909	0.963	0.405	0.045	0.393	0.508	0.140	0.081	0.119	0.042*	0.004**	0.126	0.717	0.346	0.750	0.439	0.000	0.423
T47D-CASP3	Correlation coefficient	−0.538	−0.974	0.723	0.661	−1.000	−0.829	−0.999	0.991	−0.634	−0.859	0.888	0.826	0.783	0.893	0.217	0.356	−0.871	−1.000	0.787	1.000
	Significance (2-tailed)	0.638	0.144	0.486	0.541	0.017*	0.378	0.029*	0.085	0.563	0.342	0.304	0.381	0.427	0.297	0.860	0.769	0.327	0.016*	0.423	0.000

*significant at the 0.05 level

**significant at the0.001 level

Table 6 Correlation between lncRNA expression and apoptosis parameters

		HDF-GAS5	HDF-MALAT1	HDF-p53	HDF-p27	HDF-BAX	HDF-BCL2	HDF-CASP3	MDA-GAS5	MDA-MALAT1	MDA-p53	MDA-p27	MDA-BAX	MDA-BCL2	MDA-CASP3
HDF-GAS5	Correlation coefficient	1.000	−0.410	0.384	−0.373	0.980	0.994	−0.550	−0.186	0.228	−0.016	−0.534	0.676	0.272	−0.072
	Significance (2-tailed)	0.000	0.731	0.749	0.756	0.126	0.072	0.630	0.881	0.854	0.990	0.642	0.527	0.825	0.954
HDF-MALAT1	Correlation coefficient	−0.410	1.000	0.685	0.999	−0.582	−0.510	0.987	0.972	0.794	0.918	0.990	−0.949	0.766	0.939
	Significance (2-tailed)	0.731	0.000	0.520	0.025	0.605	0.659	0.101	0.150	0.415	0.259	0.089	0.204	0.444	0.223
HDF-p53	Correlation coefficient	0.384	0.685	1.000	0.714	0.194	0.278	0.561	0.836	0.987	0.917	0.576	−0.421	0.993	0.894
	Significance (2-tailed)	0.749	0.520	0.000	0.494	0.876	0.821	0.621	0.370	0.104	0.261	0.609	0.723	0.075	0.296
HDF-p27	Correlation coefficient	−0.373	0.999	0.714	1.000	−0.549	−0.475	0.980	0.981	0.818	0.933	0.984	−0.936	0.791	0.952
	Significance (2-tailed)	0.756	0.025*	0.494	0.000	0.630	0.685	0.127	0.124	0.390	0.234	0.115	0.229	0.419	0.198
HDF-BAX	Correlation coefficient	0.980	−0.582	0.194	−0.549	1.000	0.996	−0.703	−0.376	0.032	−0.212	−0.690	0.808	0.077	−0.267
	Significance (2-tailed)	0.126	0.605	0.876	0.630	0.000	0.055*	0.503	0.755	0.980	0.864	0.515	0.401	0.951	0.828
HDF-BCL2	Correlation coefficient	0.994	−0.510	0.278	−0.475	0.996	1.000	−0.640	−0.295	0.117	−0.128	−0.625	0.755	0.162	−0.183
	Significance (2-tailed)	0.072	0.659	0.821	0.685	0.055	0.000	0.558	0.809	0.925	0.918	0.570	0.456	0.896	0.883
HDF-CASP3	Correlation coefficient	−0.550	0.987	0.561	0.980	−0.703	−0.640	1.000	0.923	0.688	0.844	1.000	−0.987	0.655	0.873
	Significance (2-tailed)	0.630	0.101	0.621	0.127	0.503	0.558	0.000	0.251	0.517	0.360	0.012*	0.102	0.546	0.325
MDA-GAS5	Correlation coefficient	−0.186	0.972	0.836	0.981	−0.376	−0.295	0.923	1.000	0.914	0.985	0.930	−0.850	0.895	0.993
	Significance (2-tailed)	0.881	0.150	0.370	0.124	0.755	0.809	0.251	0.000	0.266	0.109	0.239	0.354	0.294	0.073
MDA-MALAT1	Correlation coefficient	0.228	0.794	0.987	0.818	0.032	0.117	0.688	0.914	1.000	0.970	0.702	−0.563	0.999	0.955
	Significance (2-tailed)	0.854	0.415	0.104	0.390	0.980	0.925	0.517	0.266	0.000	0.156	0.505	0.619	0.029*	0.192
MDA-p53	Correlation coefficient	−0.016	0.918	0.917	0.933	−0.212	−0.128	0.844	0.985	0.970	1.000	0.854	−0.747	0.958	0.998
	Significance (2-tailed)	0.990	0.259	0.261	0.234	0.864	0.918	0.360	0.109	0.156	0.000	0.348	0.463	0.185	0.036*
MDA-p27	Correlation coefficient	−0.534	0.990	0.576	0.984	−0.690	−0.625	1.000	0.930	0.702	0.854	1.000	−0.984	0.669	0.882
	Significance (2-tailed)	0.642	0.089	0.609	0.115	0.515	0.570	0.012*	0.239	0.505	0.348	0.000	0.114	0.534	0.313
MDA-BAX	Correlation coefficient	0.676	−0.949	−0.421	−0.936	0.808	0.755	−0.987	−0.850	−0.563	−0.747	−0.984	1.000	−0.525	−0.784
	Significance (2-tailed)	0.527	0.204	0.723	0.229	0.401	0.456	0.102	0.354	0.619	0.463	0.114	0.000	0.648	0.427
MDA-BCL2	Correlation coefficient	0.272	0.766	0.993	0.791	0.077	0.162	0.655	0.895	0.999	0.958	0.669	−0.525	1.000	0.940
	Significance (2-tailed)	0.825	0.444	0.075	0.419	0.951	0.896	0.546	0.294	0.029*	0.185	0.534	0.648	0.000	0.221
MDA-CASP3	Correlation coefficient	−0.072	0.939	0.894	0.952	−0.267	−0.183	0.873	0.993	0.955	0.998	0.882	−0.784	0.940	1.000
	Significance (2-tailed)	0.954	0.223	0.296	0.198	0.828	0.883	0.325	0.073	0.192	0.036*	0.313	0.427	0.221	0.000

Table 6 (continued)

		HDF-GAS5	HDF-MALAT1	HDF-p53	HDF-p27	HDF-BAX	HDF-BCL2	HDF-CASP3	MDA-GAS5	MDA-MALAT1	MDA-p53	MDA-p27	MDA-BAX	MDA-BCL2	MDA-CASP3
SKBR3-GAS5	Correlation coefficient	0.794	−0.880	−0.256	−0.860	0.898	0.858	−0.944	−0.745	−0.410	−0.620	−0.938	0.985	−0.369	−0.663
	Significance (2-tailed)	0.416	0.315	0.835	0.341	0.289	0.344	0.214	0.465	0.731	0.574	0.226	0.112	0.760	0.539
SKBR3-MALAT1	Correlation coefficient	0.577	−0.982	−0.533	−0.973	0.727	0.665	−0.999	−0.910	−0.664	−0.826	−0.999	0.992	−0.629	−0.856
	Significance (2-tailed)	0.608	0.123	0.642	0.148	0.482	0.537	0.021*	0.273	0.538	0.382	0.033*	0.081	0.567	0.346
SKBR3-p53	Correlation coefficient	0.132	−0.958	−0.865	−0.969	0.325	0.242	−0.901	−0.999	−0.935	−0.993	−0.909	0.820	−0.918	−0.998
	Significance (2-tailed)	0.916	0.185	0.335	0.159	0.789	0.844	0.286	0.035*	0.231	0.074	0.274	0.388	0.260	0.038*
SKBR3-p27	Correlation coefficient	0.011	−0.916	−0.919	−0.932	0.208	0.123	−0.841	−0.985	−0.971	−1.000	−0.851	0.744	−0.959	−0.998
	Significance (2−tailed)	0.993	0.262	0.258	0.237	0.867	0.921	0.363	0.112	0.153	0.003**	0.351	0.466	0.182	0.039*
SKBR3-BAX	Correlation coefficient	−0.062	−0.885	−0.945	−0.903	0.136	0.051	−0.800	−0.969	−0.986	−0.997	−0.811	0.694	−0.977	−0.991
	Significance (2-tailed)	0.961	0.308	0.211	0.283	0.913	0.968	0.410	0.158	0.107	0.049*	0.398	0.512	0.136	0.085
SKBR3-BCL2	Correlation coefficient	0.142	−0.961	−0.860	−0.971	0.334	0.252	−0.905	−0.999	−0.931	−0.992	−0.913	0.825	−0.914	−0.998
	Significance (2-tailed)	0.909	0.178	0.341	0.153	0.783	0.838	0.280	0.028*	0.237	0.081	0.268	0.382	0.266	0.045*
SKBR3-CASP3	Correlation coefficient	0.925	−0.033	0.706	0.007	0.832	0.876	−0.191	0.202	0.581	0.366	−0.172	0.345	0.617	0.313
	Significance (2-tailed)	0.248	0.979	0.501	0.995	0.374	0.320	0.878	0.871	0.605	0.762	0.890	0.776	0.576	0.798
T47D-GAS5	Correlation coefficient	0.989	−0.269	0.518	−0.230	0.940	0.966	−0.418	−0.037	0.371	0.134	−0.401	0.558	0.413	0.078
	Significance (2-tailed)	0.096	0.827	0.654	0.852	0.222	0.167	0.725	0.977	0.758	0.914	0.737	0.623	0.729	0.950
T47D-MALAT1	Correlation coefficient	0.545	0.541	0.983	0.574	0.370	0.448	0.400	0.722	0.940	0.829	0.418	−0.249	0.955	0.797
	Significance (2-tailed)	0.633	0.636	0.117	0.611	0.759	0.704	0.738	0.486	0.221	0.377	0.726	0.840	0.192	0.413
T47D-p53	Correlation coefficient	−0.563	−0.523	−0.979	−0.557	−0.389	−0.467	−0.381	−0.707	−0.933	−0.818	−0.398	0.228	−0.948	−0.784
	Significance (2-tailed)	0.619	0.650	0.130	0.624	0.746	0.691	0.751	0.500	0.234	0.391	0.739	0.853	0.205	0.427
T47D-p27	Correlation coefficient	−0.902	0.764	0.054	0.738	−0.969	−0.944	0.857	0.593	0.216	0.447	0.847	−0.928	0.171	0.496
	Significance (2-tailed)	0.285	0.446	0.966	0.472	0.159	0.213	0.345	0.596	0.862	0.705	0.357	0.243	0.890	0.669
T47D-BAX	Correlation coefficient	−0.593	0.978	0.516	0.968	−0.740	−0.680	0.999	0.901	0.649	0.814	0.997	−0.994	0.614	0.846
	Significance (2-tailed)	0.596	0.135	0.655	0.161	0.470	0.524	0.034*	0.285	0.551	0.394	0.046*	0.069	0.579	0.358
T47D-BCL2	Correlation coefficient	−0.055	−0.888	−0.943	−0.906	0.143	0.057	−0.804	−0.971	−0.985	−0.997	−0.815	0.698	−0.976	−0.992
	Significance (2-tailed)	0.965	0.304	0.216	0.279	0.909	0.963	0.405	0.154	0.111	0.045*	0.393	0.508	0.140	0.081
T47D-CASP3	Correlation coefficient	0.572	−0.983	−0.538	−0.974	0.723	0.661	−1.000	−0.912	−0.668	−0.829	−0.999	0.991	−0.634	−0.859
	Significance (2-tailed)	0.612	0.119	0.638	0.144	0.486	0.541	0.017*	0.269	0.534	0.378	0.029*	0.085	0.563	0.342

Table 6 (continued)

		SKBR3-GAS5	SKBR3-MALAT1	SKBR3-p53	SKBR3-p27	SKBR3-BAX	SKBR3-BCL2	SKBR3-CASP3	T47D-GAS5	T47D-MALAT1	T47D-p53	T47D-p27	T47D-BAX	T47D-BCL2	T47D-CASP3
HDF-GAS5	Correlation coefficient	0.794	0.577	0.132	0.011	−0.062	0.142	0.925	0.989	0.545	−0.563	−0.902	−0.593	−0.055	0.572
	Significance (2-tailed)	0.416	0.608	0.916	0.993	0.961	0.909	0.248	0.096	0.633	0.619	0.285	0.596	0.965	0.612
HDF-MALAT1	Correlation coefficient	−0.880	−0.982	−0.958	−0.916	−0.885	−0.961	−0.033	−0.269	0.541	−0.523	0.764	0.978	−0.888	−0.983
	Significance (2-tailed)	0.315	0.123	0.185	0.262	0.308	0.178	0.979	0.827	0.636	0.650	0.446	0.135	0.304	0.119
HDF-p53	Correlation coefficient	−0.256	−0.533	−0.865	−0.919	−0.945	−0.860	0.706	0.518	0.983	−0.979	0.054	0.516	−0.943	−0.538
	Significance (2-tailed)	0.835	0.642	0.335	0.258	0.211	0.341	0.501	0.654	0.117	0.130	0.966	0.655	0.216	0.638
HDF-p27	Correlation coefficient	−0.860	−0.973	−0.969	−0.932	−0.903	−0.971	0.007	−0.230	0.574	−0.557	0.738	0.968	−0.906	−0.974
	Significance (2-tailed)	0.341	0.148	0.159	0.237	0.283	0.153	0.995	0.852	0.611	0.624	0.472	0.161	0.279	0.144
HDF-BAX	Correlation coefficient	0.898	0.727	0.325	0.208	0.136	0.334	0.832	0.940	0.370	−0.389	−0.969	−0.740	0.143	0.723
	Significance (2-tailed)	0.289	0.482	0.789	0.867	0.913	0.783	0.374	0.222	0.759	0.746	0.159	0.470	0.909	0.486
HDF-BCL2	Correlation coefficient	0.858	0.665	0.242	0.123	0.051	0.252	0.876	0.966	0.448	−0.467	−0.944	−0.680	0.057	0.661
	Significance (2-tailed)	0.344	0.537	0.844	0.921	0.968	0.838	0.320	0.167	0.704	0.691	0.213	0.524	0.963	0.541
HDF-CASP3	Correlation coefficient	−0.944	−0.999	−0.901	−0.841	−0.800	−0.905	−0.191	−0.418	0.400	−0.381	0.857	0.999	−0.804	−1.000
	Significance (2-tailed)	0.214	0.021*	0.286	0.363	0.410	0.280	0.878	0.725	0.738	0.751	0.345	0.034	0.405	0.017*

Table 6 (continued)

		SKBR3-GAS5	SKBR3-MALAT1	SKBR3-p53	SKBR3-p27	SKBR3-BAX	SKBR3-BCL2	SKBR3-CASP3	T47D-GAS5	T47D-MALAT1	T47D-p53	T47D-p27	T47D-BAX	T47D-BCL2	T47D-CASP3
MDA-GAS5	Correlation coefficient	−0.745	−0.910	−0.999	−0.985	−0.969	−0.999	0.202	−0.037	0.722	−0.707	0.593	0.901	−0.971	−0.912
	Significance (2-tailed)	0.465	0.273	0.035*	0.112	0.158	0.028*	0.871	0.977	0.486	0.500	0.596	0.285	0.154	0.269
MDA-MALAT1	Correlation coefficient	−0.410	−0.664	−0.935	−0.971	−0.986	−0.931	0.581	0.371	0.940	−0.933	0.216	0.649	−0.985	−0.668
	Significance (2-tailed)	0.731	0.538	0.231	0.153	0.107	0.237	0.605	0.758	0.221	0.234	0.862	0.551	0.111	0.534
MDA-p53	Correlation coefficient	−0.620	−0.826	−0.993	−1.000	−0.997	−0.992	0.366	0.134	0.829	−0.818	0.447	0.814	−0.997	−0.829
	Significance (2-tailed)	0.574	0.382	0.074	0.003**	0.049*	0.081	0.762	0.914	0.377	0.391	0.705	0.394	0.045*	0.378
MDA-p27	Correlation coefficient	−0.938	−0.999	−0.909	−0.851	−0.811	−0.913	−0.172	−0.401	0.418	−0.398	0.847	0.997	−0.815	−0.999
	Significance (2-tailed)	0.226	0.033*	0.274	0.351	0.398	0.268	0.890	0.737	0.726	0.739	0.357	0.046*	0.393	0.029*
MDA-BAX	Correlation coefficient	0.985	0.992	0.820	0.744	0.694	0.825	0.345	0.558	−0.249	0.228	−0.928	−0.994	0.698	0.991
	Significance (2-tailed)	0.112	0.081	0.388	0.466	0.512	0.382	0.776	0.623	0.840	0.853	0.243	0.069	0.508	0.085
MDA-BCL2	Correlation coefficient	−0.369	−0.629	−0.918	−0.959	−0.977	−0.914	0.617	0.413	0.955	−0.948	0.171	0.614	−0.976	−0.634
	Significance (2-tailed)	0.760	0.567	0.260	0.182	0.136	0.266	0.576	0.729	0.192	0.205	0.890	0.579	0.140	0.563
MDA-CASP3	Correlation coefficient	−0.663	−0.856	−0.998	−0.998	−0.991	−0.998	0.313	0.078	0.797	−0.784	0.496	0.846	−0.992	−0.859
	Significance (2-tailed)	0.539	0.346	0.038*	0.039*	0.085	0.045*	0.798	0.950	0.413	0.427	0.669	0.358	0.081	0.342

Table 6 (continued)

		SKBR3-GAS5	SKBR3-MALAT1	SKBR3-p53	SKBR3-p27	SKBR3-BAX	SKBR3-BCL2	SKBR3-CASP3	T47D-GAS5	T47D-MALAT1	T47D-p53	T47D-p27	T47D-BAX	T47D-BCL2	T47D-CASP3
SKBR3-GAS5	Correlation coefficient	1.000	0.954	0.707	0.616	0.557	0.714	0.504	0.695	−0.076	0.055	−0.979	−0.960	0.563	0.953
	Significance (2-tailed)	0.000	0.193	0.500	0.577	0.624	0.494	0.664	0.511	0.952	0.965	0.131	0.180	0.619	0.197
SKBR3-MALAT1	Correlation coefficient	0.954	1.000	0.886	0.823	0.780	0.890	0.223	0.448	−0.370	0.350	−0.874	−1.000	0.784	1.000
	Significance (2-tailed)	0.193	0.000	0.307	0.385	0.431	0.301	0.857	0.704	0.759	0.772	0.324	0.012*	0.427	0.004*
SKBR3-p53	Correlation coefficient	0.707	0.886	1.000	0.993	0.981	1.000	−0.255	−0.018	−0.759	0.745	−0.548	−0.876	0.982	0.888
	Significance (2-tailed)	0.500	0.307	0.000	0.077	0.124	0.006**	0.836	0.989	0.452	0.465	0.631	0.320	0.119	0.304
SKBR3-p27	Correlation coefficient	0.616	0.823	0.993	1.000	0.997	0.991	−0.370	−0.139	−0.832	0.820	−0.442	−0.812	0.998	0.826
	Significance (2−tailed)	0.577	0.385	0.077	0.000	0.046	0.084	0.759	0.911	0.374	0.388	0.708	0.397	0.042*	0.381
SKBR3-BAX	Correlation coefficient	0.557	0.780	0.981	0.997	1.000	0.979	−0.437	−0.210	−0.870	0.860	−0.376	−0.767	1.000	0.783
	Significance (2-tailed)	0.624	0.431	0.124	0.046*	0.000	0.130	0.712	0.865	0.328	0.341	0.754	0.443	0.004**	0.427
SKBR3-BCL2	Correlation coefficient	0.714	0.890	1.000	0.991	0.979	1.000	−0.245	−0.008	−0.752	0.738	−0.556	−0.881	0.981	0.893
	Significance (2-tailed)	0.494	0.301	0.006**	0.084	0.130	0.000	0.843	0.995	0.458	0.471	0.624	0.313	0.126	0.297
SKBR3-CASP3	Correlation coefficient	0.504	0.223	−0.255	−0.370	−0.437	−0.245	1.000	0.971	0.823	−0.835	−0.669	−0.242	−0.430	0.217
	Significance (2-tailed)	0.664	0.857	0.836	0.759	0.712	0.843	0.000	0.153	0.384	0.371	0.533	0.844	0.717	0.860

Table 6 (continued)

		SKBR3-GAS5	SKBR3-MALAT1	SKBR3-p53	SKBR3-p27	SKBR3-BAX	SKBR3-BCL2	SKBR3-CASP3	T47D-GAS5	T47D-MALAT1	T47D-p53	T47D-p27	T47D-BAX	T47D-BCL2	T47D-CASP3
T47D-GAS5	Correlation coefficient	0.695	0.448	−0.018	−0.139	−0.210	−0.008	0.971	1.000	0.665	−0.680	−0.827	−0.466	−0.204	0.443
	Significance (2-tailed)	0.511	0.704	0.989	0.911	0.865	0.995	0.153	0.000	0.537	0.524	0.380	0.692	0.869	0.708
T47D-MALAT1	Correlation coefficient	−0.076	−0.370	−0.759	−0.832	−0.870	−0.752	0.823	0.665	1.000	−1.000	−0.129	0.352	−0.867	−0.375
	Significance (2-tailed)	0.952	0.759	0.452	0.374	0.328	0.458	0.384	0.537	0.000	0.013*	0.918	0.771	0.332	0.755
T47D-p53	Correlation coefficient	0.055	0.350	0.745	0.820	0.860	0.738	−0.835	−0.680	−1.000	1.000	0.150	−0.332	0.856	0.356
	Significance (2-tailed)	0.965	0.772	0.465	0.388	0.341	0.471	0.371	0.524	0.013*	0.000	0.904	0.785	0.346	0.769
T47D-p27	Correlation coefficient	−0.979	−0.874	−0.548	−0.442	−0.376	−0.556	−0.669	−0.827	−0.129	0.150	1.000	0.883	−0.382	−0.871
	Significance (2-tailed)	0.131	0.324	0.631	0.708	0.754	0.624	0.533	0.380	0.918	0.904	0.000	0.311	0.750	0.327
T47D-BAX	Correlation coefficient	−0.960	−1.000	−0.876	−0.812	−0.767	−0.881	−0.242	−0.466	0.352	−0.332	0.883	1.000	−0.771	−1.000
	Significance (2-tailed)	0.180	0.012*	0.320	0.397	0.443	0.313	0.844	0.692	0.771	0.785	0.311	0.000	0.439	0.016*
T47D-BCL2	Correlation coefficient	0.563	0.784	0.982	0.998	1.000	0.981	−0.430	−0.204	−0.867	0.856	−0.382	−0.771	1.000	0.787
	Significance (2-tailed)	0.619	0.427	0.119	0.042*	0.004**	0.126	0.717	0.869	0.332	0.346	0.750	0.439	0.000	0.423
T47D-CASP3	Correlation coefficient	0.953	1.000	0.888	0.826	0.783	0.893	0.217	0.443	−0.375	0.356	−0.871	−1.000	0.787	1.000
	Significance (2-tailed)	0.197	0.004**	0.304	0.381	0.427	0.297	0.860	0.708	0.755	0.769	0.327	0.016*	0.423	0.000

*significant at the 0.05 level

**significant at the0.001 level

Discussion

Cancer is believed to be one of the chief causes of death all around the globe. Undoubtedly, cancer patients' care has been improved by the approach of modern drug-targeted therapeutics. However, advanced metastasized cancer is still untreatable. Therefore, it is necessary for look for a reliable and more efficient chemoprevention and treatment to develop the facilities and reduce treatment costs for cancer care. Cancer chemoprevention with natural phytochemical compounds is a novel technique for preventing and curing cancer (Wang et al. 2012). In the present study, our research groups have biosynthesized the stable and cost-effective CM-Cu_2O NPs. The synthesis of crystalline CM-Cu_2O NPs were confirmed by various analytical techniques like UV–Vis, FTIR, XRD and SEM. Further the synthesized CM-Cu_2O NPs were screened for anticancer activity on BC cell lines by MTT assay. The obtained result inferred that the synthesized CM-Cu_2O NPs demonstrated high anticancer cytotoxicity on BC cell lines (MDA, SKBR and T47D).

Copper oxide nanoparticles are applied increasingly for various purposes like antimicrobial preparations, heat transfer fluids, semiconductors or intrauterine contraceptive devices (Chen et al. 2011). Copper oxide nanoparticles have two key forms including CuO and Cu_2O. Some studies have shown the toxic influence of CuO associated with the production of reactive oxygen species (ROS), lipid peroxidation, and DNA damage (Fahmy and Cormier 2009) except for Cu_2O. Thus, it is essential to investigate the toxicity of Cu_2O NP that is believed to be a source of water-borne copper-containing species (Singh and Turner 2009). The solubility of nanoparticles is dangerous for the toxicity of these particles and their influences on ecosystems (Midander et al. 2009). Yet, some studies reported that higher stability could help the nanoparticles for penetrating, accumulating and persisting to a large extent in an organism (Midander et al. 2009). However, it is still not clear as to what extent the toxicity of particles can be ascribed to the soluble or released metal fraction or by the specific particle. It is believed that in the mechanism of the toxicity of CuNPs, the cellular membrane is ruptured (Karlsson et al. 2013). Because there is a higher O2 concentration in the cell membrane compared to the cell media, CuNPs are oxidized as they go through the cell membrane, producing copper ions. Thus, the cellular rupture could be the result of the metal release process into the cell, which results in the production of H2O2 locally at the cell membrane (Vanwinkle et al. 2009). Note that rupturing of the cellular membrane is not only caused by the released copper ion into the cell, but also is brought about by the direct exposure of human alveolar epithelial cell line A549 to the copper ions resulting in less toxic damage to the membrane (Karlsson et al. 2008; Midander et al. 2009). Note that copper ion release process from CuNPs into the vicinity of membrane surface is a serious stage in CuNPs toxicity. Other studies have used carbon-coated CuNPs and $CuCl_2$, both of which did not bring about membrane rupture, while CuNPs induced rupturing of the cell membrane (Minocha and Mumper 2012). It could be said that the ultimate fate of Cu-metal nanoparticles after going into the body is degradation and production of Cu2 + ions. Thus, after exerting their cytotoxic effect on cancer cell and being released as ions, they will not be cytotoxic, since Cu2 + ion is not cytotoxic in concentrations lower than 500 μM.

Apoptosis or cell suicide is a highly regulated process happening in almost all living cells. In apoptosis, a series of molecular events is activated that results in cell death characterized by cellular, morphological and biochemical variations including cell shrinkage, chromatin condensation and nuclear fragmentation, membrane blebbing, caspase activation, and the formation of membrane bound vesicles termed as apoptotic bodies (Balachandran et al. 2014). Two key pathways are involve in apoptosis. The first, called the extrinsic or cytoplasmic pathway, is activated through the Fas death receptor, a member of the tumor necrosis factor (TNF) receptor superfamily (Zapata et al. 2001). The second pathway is the intrinsic or mitochondrial pathway that when stimulated results in the release of cytochrome c from the mitochondria and activation of the death signal (Hockenbery et al. 1990). Both pathways converge to a final common pathway and trigger a cascade of proteases called caspases that cleave regulatory and structural molecules, terminating in the death of the cell. The main pathway resulting in the execution of the death signal is the activation of a series of proteases termed caspases. Not all caspases play a role in apoptosis. Caspases are cysteine-aspartic proteases families involved significantly in apoptosis, necrosis and inflammation. Caspases are regulated at a post-translational level making certain that they can be quickly triggered. The caspases implicated in apoptosis can be further categorized into two functional subgroups according to their known or hypothetical roles in the process: initiator caspase (caspases-2, -8, -9, and -10) and effector caspases (caspases-3, -6, and -7). The caspases that have been well described are caspases-3, -6, -7, -8 and -9 (Mancini et al. 1998). Caspase-3 is considered as a key protease triggered during the early stages of apoptosis (Walsh et al. 2008). Caspases are triggered in a sequential cascade of cleavages from their inactive forms and the active caspase-3 proteolytically cleaves and triggers other caspases and other relevant target molecules in the cytoplasm or nucleus (Brentnall et al. 2013; Walsh et al. 2008). The process of cell death could involve discharging cytochrome c from the mitochondria leading consequently to apoptosis through triggering the caspases. Together, these data recommend a linear and specific activation cascade between caspase-9 and caspase-3 in response to cytochrome c discharged from the mitochondria (Shalini et al. 2015). Activation of caspase-9, in turn, cleaves effector caspases such as caspase-3, -6, and -7 (Porter and Jänicke 1999; Shalini et al. 2015). Then the effector caspases cleave their target proteins and culminate in the systematic death of the cell. In this pathway of apoptosis, caspase-3 and caspase-9 could be the key factors, since their activities affects the process of apoptosis as well as the cell death type (Balachandran et al. 2014). Caspase-3 then could be capable of cleaving a series of proteins such as PARP, a DNA repair enzyme, nuclear lamins, gelsolin, and fodrin (Chang and Yang 2003). In the mitochondria, the tBid efficiently triggers *Bax*, leading to the release of cytochrome c and mitochondrial dysfunction. This alternative is a crosstalk between the receptor and mitochondria mediated pathways that is capable of amplifying the caspase activation required for apoptosis. Actually, more recent studies have turned their attention to multiple signal transduction cascades activating cells to experience apoptosis (Lockshin and Zakeri 2004). Caspase 3 is a potential marker to predict response or resistance to chemotherapeutic agents in BC (O'Donovan et al. 2003). In fact, recent data from BC cell lines confirm this hypothesis.

For instance, Blanc et al. (2000) argued that caspase 3 was necessary for procaspase 9 processing and cisplatin-induced apoptosis in MCF7 BC cells. Applying the same cell lines, Yang et al.(Yang et al. 2001) showed that transfection with cDNA for caspase 3 resulted in doxorubicin- and etoposide-induced apoptosis. In comparison with other genes involved in apoptosis (e.g., *p53* and the Bcl-2 family), studies on caspase expression in BC are scarce.

It is believed that *p27* is an important factor of the G_1- to S-phase transition in the cell cycle that is involved in tumor progression (Matsunobu et al. 2004). *P27* is a member of the Cip/Kip family of cyclin-dependent kinase inhibitors present at high levels in quiescent cells (Sherr and Roberts 1995). The gene encoding *p27* is seldom mutated; however, *p27* is functionally inactivated in most human cancers through improved *p27* proteolysis, through sequestration by cyclin D/cyclin-dependent kinase complexes, and by cytoplasmic mislocalization (Filipits et al. 2009). Guan et al. (2010) reported that further studies were required to shed light on the role of cytoplasmic *p27* in BC. Porter et al. (1997) assayed both *p27* and cyclin E levels in 246 primary BC of women under 45 years of age. Patients whose BCs showed both low *p27* and elevated cyclin E proteins had the highest mortality, and multivariate analysis demonstrated that both levels of *p27* and cyclin E were independent predictors of overall survival. Tan et al. (1997) reported that the prognostic value of *p27* in 202 patients with BCs was less than 1 cm in size (T1a,b) in comparison with clinicopathological features and other parameters such as *p53*, c-erb-B2, Ki-67, cdc25B, and the density of microvessels. This study revealed that low *p27* level, established as less than 50% of the tumor cells being positive for *p27*, was not a dependent risk factor on multivariate analysis and was linked to a 3.4-fold increased risk of death, especially in node-negative tumors. The *p53* tumor suppressor gene inhibits tumourigenesis in response to physiological and environmental stress and is involved in cell cycle progression, apoptosis and repair of DNA damage. *P53* may play a role in transcriptional regulation of pro-apoptotic genes linked to intrinsic and extrinsic pathways (Liu et al. 2014). Triggered *p53* increases the expression of p21 in DNA damaged cells and influences expression of *p27* (Balachandran et al. 2014). The loss of the *p53* function shows the most common genetic change known in human cancers. Haldar et al. argued the down-regulation of Bcl-2 at both the protein and mRNA levels was induced due to the overexpression of mutant *p53* in BC (MCF-7) cell line (Haldar et al. 1994). Some studies have confirmed the involvement of Bcl-2 in the control of apoptosis; recent experimental studies have confirmed that Bcl-2 is implicated in regulating the cell cycle and proliferation (Bonnefoy-Berard et al. 2004). The Bcl-2 deficient T cells showed an accelerated cell cycle progression (Linette et al. 2002). However, the cells overexpressing the Bcl-2 gene product not only revealed a delayed start of apoptosis but also a quick arrest in the G1 phase of the cell cycle (Marvel et al. 1994) indicating that Bcl-2 is involved in the transition from G0/G1 to S phase (Bonnefoy-Berard et al. 2004). Vairo et al. also confirmed the Bcl-2 hindered the cell cycle entry by increasing the *p27* and p130 levels (Vairo et al. 2000). Greider et al. reported that Bcl-2 could not hinder the S phase entry in *p27* null cells indicating that *p27* is necessary for the cell cycle regulation of Bcl-2 (Greider et al. 2002). According to these experimental findings, Bcl-2 directly increased the level of *p27* (Greider et al. 2002; Linette et al. 2002; Marvel et al. 1994), thus regulating the cell cycle and progression (Bonnefoy-Berard et al. 2004). Triggering *p53* induces up-regulation of pro-apoptotic *Bax* but not anti-apoptotic Bcl-2. *P53* mediated apoptosis play a role in triggering Fas and the intrinsic mitochondrial pathway leading to the activation of caspases-8 and -9 (Liebermann et al. 2007). Now, the cancer biology requires identifying new active chemotherapy drugs capable of acting as lead compounds for effective drug development. Thus, the BCL2/*BAX* ratio within a cell is a critical determinant of apoptosis and a reduced BCL2/*BAX* ratio is a factor causing endometrial cells susceptible to apoptosis. Some studies believe that dysfunction of the *p53*/BCL2/*BAX* apoptosis signaling pathway is involved in tumorigenesis and tumor progression (Argiris et al. 2006; Vaskivuo et al. 2000).

In this study, we examined the expression of apoptosis genes (*p53, p27, bax, bcl2* and *caspase3*) in MDA-MB-231, SKBR3 and T-47D BC cell lines compared to HDF control cell line. The results revealed that *p53, p27, bax* and *caspase3* were significantly upregulated in BC cell lines as compared with normal cell line (Fig. 7). On the other hand, *bcl2* expression was also significantly increased in MDA-MB-231 and T47D cell lines compared with normal cell line, but *bcl2* levels were downregulated in SKBR3 cell line. As a limitation of our study, differential expression in protein for *p53, p27, bax, bcl2* and *caspase3*, which may reduce the accuracy of the results. A main reason for the application of a cytotoxic chemotherapeutic agent is its potential for inducing apoptosis and cell death in cancer cells (Hannun et al. 1997), because during apoptosis, the cells die with no inflammatory responses (Satchell et al. 2003). Statistics show that BC has developed uncontrollably necessitating the discovery and development of a novel anticancer agent having less side effects for normal cells (Parkin et al. 2009).

lncRNAs have been brought to light lately because of their confirmed involvement in the molecular pathobiology of several cancers (Zhao et al. 2014). BC has been observed in women of different ages, but that affecting younger women is of poorer prognosis (Santos et al. 2014). The present study assessed the expression levels of two lncRNAs, i.e., *MALAT1* and *GAS5* in the MDA-MB-231, SKBR3 and T-47D BC cell lines. According to our expression analyses, *MALAT1* was upregulated, while *GAS5* was downregulated in cell lines (Fig. 8). As discussed above, some studies have confirmed poorer prognosis for BC (Arshi et al. 2018). Some studies have shown that *GAS5* has a tumor-suppressive role by controlling mammalian cell apoptosis, and its downregulation is reportedly is involved in tumor formation (Mourtada-Maarabouni et al. 2009). Moreover, there is a link between *GAS5* low expression levels and a poor prognosis in head and neck squamous cell carcinoma (Gee et al. 2011). Thus, our finding of significant *GAS5* downregulation in SKBR3 and T-47D cell lines tested compared to HDF cell line may explain the molecular mechanism causing a poorer prognosis of BC in this age group.

Conclusions

It was shown in this study that the leaves of Cystoseira myrica can be an unconventional resource for the green synthesis of CM-Cu_2O NPs. The analytical techniques like UV–Vis, XRD, TEM and SEM were applied to characterize the nature of the synthesized

CM-Cu_2O NPs. It was also shown that the CM-Cu_2O NPs synthesized from the leaves of Cystoseira myrica have significant anticancer activity in BC cell lines. Moreover, identifying and isolating the biologically active compound from the leaves extract of Cystoseira myrica could facilitate the discovery of novel anticancer drug. The superior effectiveness and lower toxicity of new anticancer drug are mostly because of applying nanosized Cu_2O based drug designing molecules. According to new studies, various natural products are capable of inducing the apoptosis of cancer cells, and inhibiting metastasis and tumor cell growth highlighting the application and advantage of these natural compounds as of new medical treatment of human cancer. According to in vitro studies, CM-Cu_2O NPs, which is commonly used among current cell lines utilize in this study, is an anticancer substance with proapoptotic characteristics in terms of human cancer cells. Our study obviously showed that CM-Cu_2O NPs alters the expression level of some critical genes in various human cancer cells. These findings show that CM-Cu_2O NPs could probably be used as a therapeutic anticancer drug. Previous research works and the data in our analysis show that dysregulation of lncRNA expression is a main component in the tumorigenesis process. Yet, the expression pattern of these RNAs is different in various BC cell lines, an idea shedding light on the significance of considering the variable pathobiology of tumors upon the application of therapeutic approaches. Accordingly, the present study particularly revealed that lncRNAs evaluated in this study show different levels of expression in BCs developed in BC cell lines compared to normal cell line. Specifically, previous studies supported the fact that different expression of one of these differentially expressed lncRNAs, i.e., *GAS5*, could shed light on the worse result of BC in patients at molecular levels. These findings can also be used to define future therapeutic regimens.

Abbreviations

GAPDH: Glyceraldehyde-3-Phosphate Dehydrogenase; qRT-PCR: Quantitative reverse transcription polymerase chain reaction; LncRNAs: Long noncoding RNAs; Cu_2O: Cuprous oxide; BC: Breast cancer; CM-Cu_2O NPs: Cystoseira myrica algae nanoparticles; FTIR: Fourier transform infrared spectroscopy; XRD: X-ray diffraction; SEM: Scanning electron microscopy; CR: Circadian rhythm; ER: Endoplasmic reticulum; GAS5: Growth arrest-specific 5; MALAT1: Metastasis Associated Lung Adenocarcinoma Transcript 1; TSSs: Transcription start sites; $CuCl_2$: Copper chloride; ELISA: Enzyme-linked immunosorbent assay.

Acknowledgements

The authors would like to thank the staff members of Biotechnology Research Center of Islamic Azad University, Shahrekord Branch, Iran for their help and support.

Authors' contributions

PT and MC collected the related reports and drafted the manuscript. MC revised the manuscript. MC participated in designing the review. Both authors read and approved the final manuscript.

Funding

The authors received no funding from an external source.

Availability of data and materials

Not applicable.

Ethics approval and consent to participate

Not applicable.

Consent for publication

Not applicable.

Competing interests

The authors declare that they have no competing interests.

Received: 2 July 2020 Accepted: 27 September 2020
Published online: 14 October 2020

References

Abudayyak M, Guzel E, Özhan G. Cupric oxide nanoparticles induce cellular toxicity in liver and intestine cell lines. Adv Pharm Bull. 2020;10:213–220. https://doi.org/10.34172/apb.2020.025
Ahmad T, Wani IA, Manzoor N, Ahmed J, Asiri AM. Biosynthesis, structural characterization and antimicrobial activity of gold and silver nanoparticles. Colloids Surf B Biointerfaces. 2013;107:227–34.
Arafat WO, Gómez-Navarro J, Xiang J, Barnes MN, Mahasreshti P, Alvarez RD, et al. An adenovirus encoding proapoptotic Bax induces apoptosis and enhances the radiation effect in human ovarian cancer. Mol Ther. 2000;1:545–54.
Argiris A, Cohen E, Karrison T, Esparaz B, Mauer A, Ansari R, et al. A phase II trial of perifosine, an oral alkylphospholipid, in recurrent or metastatic head and neck cancer. Cancer Biol Ther. 2006;5(7):766–70.
Arshi A, Sharifi FS, Khorramian Ghahfarokhi M, Faghih Z, Doosti A, Ostovari S, et al. Expression analysis of MALAT1, GAS5, SRA, and NEAT1 lncRNAs in breast cancer tissues from young women and women over 45 years of age. Mol Ther Nucleic Acids. 2018;12:751–7.
Asadzadeh Vostakolaei F, Broeders MJM, Mousavi SM, Kiemeney LALM, Verbeek ALM. The effect of demographic and lifestyle changes on the burden of breast cancer in Iranian women: a projection to 2030. Breast. 2013;22(3):277–81.
Balachandran C, Sangeetha B, Duraipandiyan V, Raj MK, Ignacimuthu S, Al-Dhabi NA, et al. A flavonoid isolated from Streptomyces sp (ERINLG-4) induces apoptosis in human lung cancer A549 cells through p53 and cytochrome c release caspase dependant pathway. Chem Biol Interact. 2014;224:24–35.
Bednorz JG, Müller KA. Possible high Tc superconductivity in the Ba-La-Cu-O system. Zeitschrift für Phys B Condens Matter. 1986;64(2):189–93.
Bernard D, Prasanth KV, Tripathi V, Colasse S, Nakamura T, Xuan Z, et al. A long nuclear-retained non-coding RNA regulates synaptogenesis by modulating gene expression. EMBO J. 2010;29(18):3082–93.
Blanc C, Deveraux QL, Krajewski S, Jänicke RU, Porter AG, Reed JC, et al. Caspase-3 is essential for procaspase-9 processing and cisplatin-induced apoptosis of MCF-7 breast cancer cells. Cancer Res. 2000;60(16):4386–90.
Bonnefoy-Berard N, Aouacheria A, Verschelde C, Quemeneur L, Marçais A, Marvel J. Control of proliferation by Bcl-2 family members. Biochim Biophys Acta Mol Cell Res. 2004;1644(2–3):159–68.
Borkow G, Gabbay J. Copper, an ancient remedy returning to fight microbial, fungal and viral infections. Curr Chem Biol. 2012;3(3):272–8.
Borkow G, Zatcoff RC, Gabbay J. Reducing the risk of skin pathologies in diabetics by using copper impregnated socks. Med Hypotheses. 2009;73(6):883–6.
Brentnall M, Rodriguez-Menocal L, De Guevara RL, Cepero E, Boise LH. Caspase-9, caspase-3 and caspase-7 have distinct roles during intrinsic apoptosis. BMC Cell Biol. 2013;14(1):32.
Brimmell M, Mendiola R, Mangion J, Packham G. BAX frameshift mutations in cell lines derived from human haemopoietic malignancies are associated with resistance to apoptosis and microsatellite instability. Oncogene. 1998;16(14):1803–12.
Carnes CL, Stipp J, Klabunde KJ, Bonevich J. Synthesis, characterization, and adsorption studies of nanocrystalline copper oxide and nickel oxide. Langmuir. 2002;18(4):1352–9.
Chang HY, Yang X. Proteases for cell auicide: functions and regulation of caspases. Microbiol Mol Biol Rev. 2003;64(4):821–46.
Chen D, Zhang D, Yu JC, Chan KM. Effects of Cu_2O nanoparticle and $CuCl_2$ on zebrafish larvae and a liver cell-line. Aquat Toxicol. 2011;105(3–4):344–54.
Davoodi H, Hashemi SR, Seow HF. 5-Fluorouracil induce the expression of TLR4 on HCT116 colorectal cancer cell line expressing different variants of TLR4. Iran J Pharm Res. 2013;12(2):453.
Delbridge ARD, Strasser A. The BCL-2 protein family, BH3-mimetics and cancer therapy. Cell Death Differ. 2015;22(7):1071–80.
Dibra D, Mitra A, Newman M, Xia X, Cutrera JJ, Gagea M, et al. Lack of immunomodulatory interleukin-27 enhances oncogenic properties of mutant p53 in vivo. Clin Cancer Res. 2016;22(15):3876–83.
Erdem JS, Notø HØ, Skare Ø, Lie JAS, Petersen-øverleir M, Reszka E, et al. Mechanisms of breast cancer risk in shift workers: association of telomere shortening with the duration and intensity of night work. Cancer Med. 2017a;6(8):1988–97.
Erdem JS, Skare Ø, Petersen-Øverleir M, Notø HØ, Lie JAS, Reszka E, et al. Mechanisms of breast cancer in shift workers: DNA methylation in five core circadian genes in nurses working night shifts. J Cancer. 2017b;8(15):2876.
Fahmy B, Cormier SA. Copper oxide nanoparticles induce oxidative stress and cytotoxicity in airway epithelial cells. Toxicol. Vitr. 2009;23(7):1365–71.
Filipits M, Rudas M, Heinzl H, Jakesz R, Kubista E, Lax S, et al. Low p27 expression predicts early relapse and death in postmenopausal hormone receptor-positive breast cancer patients receiving adjuvant tamoxifen therapy. Clin Cancer Res. 2009;15(18):5888–94.
Gee HE, Buffa FM, Camps C, Ramachandran A, Leek R, Taylor M, et al. The small-nucleolar RNAs commonly used for microRNA normalisation correlate with tumour pathology and prognosis. Br J Cancer. 2011;104(7):1168–77.
Ghidan AY, Al-Antary TM, Awwad AM. Green synthesis of copper oxide nanoparticles using Punica granatum peels extract: Effect on green peach Aphid. Environ Nanotechnology Monit Manag. 2016;6:95–8.
Gnanavel V, Palanichamy V, Roopan SM. Biosynthesis and characterization of copper oxide nanoparticles and its anticancer activity on human colon cancer cell lines (HCT-116). J Photochem Photobiol B Biol. 2017;171:133–8.

Greider C, Chattopadhyay A, Parkhurst C, Yang E. BCL-xL and BCL2 delay Myc-induced cell cycle entry through elevation of p27 and inhibition of G1 cyclin-dependent kinases. Oncogene. 2002;21(51):7765–75.

Guan X, Wang Y, Xie R, Chen L, Bai J, Lu J, et al. P27Kip1 as a prognostic factor in breast cancer: a systematic review and meta-analysis. J Cell Mol Med. 2010;14(4):944–53.

Haldar S, Negrini M, Monne M, Sabbioni S, Croce CM. Down-Regulation of bcl-2 by p53 in breast cancer cells. Cancer Res. 1994;54(8):2095–7.

Hannun YA, Cress A, Hazlehurst L, Shtil A, Dalton W, Bhalla K. Apoptosis and the dilemma of cancer chemotherapy. Blood. 1997;89(6):1845–53.

Hockenbery D, Nuñez G, Milliman C, Schreiber RD, Korsmeyer SJ. Bcl-2 is an inner mitochondrial membrane protein that blocks programmed cell death. Nature. 1990;348(6299):334–6.

Hrdlickova B, de Almeida RC, Borek Z, Withoff S. Genetic variation in the non-coding genome: involvement of micro-RNAs and long non-coding RNAs in disease. Biochim Biophys Acta Mol Basis Dis. 2014;1842(10):1910–22.

Ishihara T, Higuchi M, Takagi T, Ito M, Nishiguchi H, Takita Y. Preparation of CuO thin films on porous BaTiO3by self-assembled multibilayer film formation and application as a CO2sensor. J Mater Chem. 1998;8(9):2037–42.

Ji P, Diederichs S, Wang W, Böing S, Metzger R, Schneider PM, et al. MALAT-1, a novel noncoding RNA, and thymosin β4 predict metastasis and survival in early-stage non-small cell lung cancer. Oncogene. 2003;22(39):8031–41.

Karlsson HL, Cronholm P, Gustafsson J, Möller L. Copper oxide nanoparticles are highly toxic: a comparison between metal oxide nanoparticles and carbon nanotubes. Chem Res Toxicol. 2008;21(9):1726–32.

Karlsson HL, Cronholm P, Hedberg Y, Tornberg M, De Battice L, Svedhem S, et al. Cell membrane damage and protein interaction induced by copper containing nanoparticles-Importance of the metal release process. Toxicology. 2013;313(1):59–69.

Katner AL, Hoang QBL, Gootam P, Jaruga E, Ma Q, Gnarra J, et al. Induction of cell cycle arrest and apoptosis in human prostate carcinoma cells by a recombinant adenovirus expressing p27Kip1. Prostate. 2002;53(1):77–87.

Kumar R, Roopan SM, Prabhakarn A, Khanna VG, Chakroborty S. Agricultural waste Annona squamosa peel extract: biosynthesis of silver nanoparticles. Spectrochim Acta Part A Mol Biomol Spectrosc. 2012;90:173–6.

Kumar MD, John KMM, Karthik S. The bone fracture-healing potential of ormocarpum cochinchinense, methanolic extract on albino wistar rats. J Herbs Spices Med Plants. 2013;19(1):1.

Kumar PPNV, Shameem U, Kollu P, Kalyani RL, Pammi SVN. Green synthesis of copper oxide nanoparticles using aloe vera leaf extract and its antibacterial activity against fish bacterial pathogens. Bionanoscience. 2015;5(3):135–9.

Lie JAS, Kjuus H, Zienolddiny S, Haugen A, Stevens RG, Kjærheim K. Night work and breast cancer risk among norwegian nurses: assessment by different exposure metrics. Am J Epidemiol. 2011;173(11):1272–9.

Liebermann DA, Hoffman B, Vesely D. p53 induced growth arrest versus apoptosis and its modulation by survival cytokines. Cell Cycle. 2007;6(2):166–70.

Linette GP, Li Y, Roth K, Korsmeyer SJ. Cross talk between cell death and cell cycle progression: BCL-2 regulates NFAT-mediated activation. Proc Natl Acad Sci. 2002;93(18):9545–52.

Liu J, Zhang C, Feng Z. Tumor suppressor p53 and its gain-of-function mutants in cancer. Acta Biochim Biophys Sin. 2014;46(3):170–9.

Lockshin RA, Zakeri Z. Caspase-independent cell death? Oncogene. 2004;23(16):2766–73.

Malandrino G, Condorelli GG, Lanza G, Fragalà IL, Scotti Di Uccio U, Valentino M. Effect of Ba-Ca-Cu precursor matrix on the formation and properties of superconducting Tl2Ba2Can-1CunOx films: a combined metalorganic chemical vapour deposition and thallium vapour diffusion approach. J Alloys Compd. 1997;251(1–2):332–6.

Mancini M, Nicholson DW, Roy S, Thornberry NA, Peterson EP, Casciola-Rosen LA, et al. The caspase-3 precursor has a cytosolic and mitochondrial distribution: implications for apoptotic signaling. J Cell Biol. 1998;140(6):1485–95.

Marvel J, Perkins GR, Lopez Rivas A, Collins MK. Growth factor starvation of bcl-2 overexpressing murine bone marrow cells induced refractoriness to IL-3 stimulation of proliferation. Oncogene. 1994;9(4):1117.

Matsumoto Y, Tanaka K, Nakatani F, Matsunobu T, Matsuda S, Iwamoto Y. Downregulation and forced expression of EWS-Fli1 fusion gene results in changes in the expression of G1 regulatory genes. Br J Cancer. 2001;84(6):768–75.

Matsunobu T, Tanaka K, Matsumoto Y, Nakatani F, Sakimura R, Hanada M, et al. The prognostic and therapeutic relevance of p27kip1 in Ewing's family tumors. Clin Cancer Res. 2004;10(3):1003–12.

Midander K, Cronholm P, Karlsson HL, Elihn K, Möller L, Leygraf C, et al. Surface characteristics, copper release, and toxicity of nano- and micrometer-sized copper and copper(II) oxide particles: a cross-disciplinary study. Small. 2009;5(3):389–99.

Minocha S, Mumper RJ. Effect of carbon coating on the physico-chemical properties and toxicity of copper and nickel nanoparticles. Small. 2012;8(21):3289–99.

Mourtada-Maarabouni M, Pickard MR, Hedge VL, Farzaneh F, Williams GT. GAS5, a non-protein-coding RNA, controls apoptosis and is downregulated in breast cancer. Oncogene. 2009;28(2):195–208.

Mousavi SM, Zheng T, Dasteiri S, Miller AB. Age distribution of breast cancer in the middle east, implications for screening. Breast J. 2009;15(6):677–9.

Naddafi K, Saeedi R. Biosorption of copper(II) from aqueous solutions by brown macroalga Cystoseira myrica biomass. Environ Eng Sci. 2009;26(5):1009–15.

Nakayama K, Ishida N, Shirane M, Inomata A, Inoue T, Shishido N, et al. Mice lacking p27Kip1 display increased body size, multiple organ hyperplasia, retinal dysplasia, and pituitary tumors. Cell. 1996;85(5):707–20.

Nishimoto Y, Nakagawa S, Hirose T, Okano HJ, Takao M, Shibata S, et al. The long non-coding RNA nuclear-enriched abundant transcript 1-2 induces paraspeckle formation in the motor neuron during the early phase of amyotrophic lateral sclerosis. Mol. Brain. 2013;6(1):1–8.

O'Donovan N, Crown J, Stunell H, Hill ADK, McDermott E, O'Higgins N, et al. Caspase 3 in breast cancer. Clin Cancer Res. 2003;9(2):738–42.

Oltval ZN, Milliman CL, Korsmeyer SJ. Bcl-2 heterodimerizes in vivo with a conserved homolog, Bax, that accelerates programed cell death. Cell. 1993;74(4):609–19.

Parashar V, Parashar R, Sharma B, Pandey AC. Parthenium leaf extract mediated synthesis of silver nanoparticles: A novel approach towards weed utilization. Dig. J. Nanomater. Biostructures. 2009.

Parkin DM, Bray F, Ferlay J, Pisani P. Global Cancer Statistics, 2002. CA Cancer J Clin. 2009;55(2):74–108.

Porter AG, Jänicke RU. Emerging roles of caspase-3 in apoptosis. Cell Death Differ. 1999;6(2):99–104.

Porter PL, Malone KE, Heagerty PJ, Alexander GM, Gatti LA, Firpo EJ, et al. Expression of cell-cycle regulators p27(Kip1) and cyclin E, alone and in combination, correlate with survival in young breast cancer patients. Nat Med. 1997;3(2):222–5.

Raho G, Barone V, Rossi D, Philipson L, Sorrentino V. The gas 5 gene shows four alternative splicing patterns without coding for a protein. Gene. 2000;256(1–2):13–7.

Rasmussen JW, Martinez E, Louka P, Wingett DG. Zinc oxide nanoparticles for selective destruction of tumor cells and potential for drug delivery applications. Expert Opin Drug Deliv. 2010;7(9):1063–77.

Roopan SM, Kumar SHS, Madhumitha G, Suthindhiran K. Biogenic-Production of SnO_2 Nanoparticles and Its Cytotoxic Effect Against Hepatocellular Carcinoma Cell Line (HepG2). Appl Biochem Biotechnol. 2014;175(3):1567–75.

Sakakura C, Sweeney EA, Shirahama T, Igarashi Y, Hakomori SI, Nakatani H, et al. Overexpression of bax sensitizes human breast cancer MCF-7 cells to radiation-induced apoptosis. Int J Cancer. 1996;67(1):101–5.

Santos SS, Melo LR, Koifman RJ, Koifman S. Breast cancer incidence and mortality in women under 50 years of age in Brazil. Cad Saude Publica. 2014;29(11):2230–40.

Sapkota Y, Mackey JR, Lai R, Franco-Villalobos C, Lupichuk S, Robson PJ, et al. Assessing SNP–SNP interactions among DNA repair, modification and metabolism related pathway genes in breast cancer susceptibility. PLoS ONE. 2013;8(6):e64896.

Satchell PG, Gutmann JL, Witherspoon DE. Apoptosis: an introduction for the endodontist. Int Endod J. 2003;25(9):888–96.

Schneider C, King RM, Philipson L. Genes specifically expressed at growth arrest of mammalian cells. Cell. 1988;54(6):787–93.

Shalini S, Dorstyn L, Dawar S, Kumar S. Old, new and emerging functions of caspases. Cell Death Differ. 2015;22(4):526–39.

Sherr CJ, Roberts JM. Inhibitors of mammalian G1 cyclin-dependent kinases. Genes Dev. 1995;9(10):1149–63.

Siegel R, Naishadham D, Jemal A. Cancer statistics, 2013 (US). CA Cancer J Clin. 2013;62(1):10–29.

Singh N, Turner A. Leaching of copper and zinc from spent antifouling paint particles. Environ Pollut. 2009;157(2):371–6.

Smith CM, Steitz JA. Classification of gas5 as a multi-small-nucleolar-RNA (snoRNA) host gene and a member of the 5′-terminal oligopyrimidine gene family reveals common features of snoRNA host genes. Mol Cell Biol. 2015;18(12):6897–909.

Stennicke HR, Salvesen GS. Properties of the caspases. Biochim Biophys Acta Protein Struct Mol Enzymol. 1998;1387(1–2):17–31.

Tan P, Cady B, Wanner M, Worland P, Cukor B, Magi-Galluzzi C, et al. The cell cycle inhibitor p27 is an independent prognostic marker in small (T(1a, b)) invasive breast carcinomas. Cancer Res. 1997;57(7):1259–63.

Thandapani P, Aifantis I. Apoptosis, Up the Ante. Cancer Cell. 2017;32(4):402–3.

Tripathi V, Ellis JD, Shen Z, Song DY, Pan Q, Watt AT, et al. The nuclear-retained noncoding RNA MALAT1 regulates alternative splicing by modulating SR splicing factor phosphorylation. Mol Cell. 2010;39(6):925–38.

Vairo G, Soos TJ, Upton TM, Zalvide J, DeCaprio J, Ewen ME, et al. Bcl-2 retards cell cycle entry through p27(Kip1), pRB relative p130, and altered E2F regulation. Mol Cell Biol. 2000;20(13):4745–53.

Van Grembergen O, Bizet M, De Bony EJ, Calonne E, Putmans P, Brohée S, et al. Portraying breast cancers with long noncoding RNAs. Sci Adv. 2016;2(9):e1600220.

Vanden Berghe DA, Vlietinck AJ, Dey DM, Harborne JB. screening methods for antibacterial and antiviral agents from higher plants. Assays for Bioactivity. 1991.

Vanwinkle BA, De Mesy Bentley KL, Malecki JM, Gunter KK, Evans IM, Elder A, et al. Nanoparticle (NP) uptake by type i alveolar epithelial cells and their oxidant stress response. Nanotoxicology. 2009;3(4):307–18.

Vaskivuo TE, Stenbäck F, Karhumaa P, Risteli J, Dunkel L, Tapanainen JS. Apoptosis and apoptosis-related proteins in human endometrium. Mol Cell Endocrinol. 2000;165(1–2):75–83.

Vijay Kumar R, Elgamiel R, Diamant Y, Gedanken A, Norwig J. Sonochemical preparation and characterization of nanocrystalline copper oxide embedded in poly(vinyl alcohol) and its effect on crystal growth of copper oxide. Langmuir. 2001;17(5):1406–10.

Vinardell M, Mitjans M. Antitumor activities of metal oxide nanoparticles. Nanomaterials. 2015;5(2):1004–21.

Vostakolaei FA, Broeders MJM, Rostami N, Feuth T, van Dijck JAAM, Verbeek ALM, et al. Age at diagnosis and breast cancer survival in Iran. Int J Breast Cancer. 2012;2012:1–8.

Walsh JG, Cullen SP, Sheridan C, Lüthi AU, Gerner C, Martin SJ. Executioner caspase-3 and caspase-7 are functionally distinct proteases. Proc Natl Acad Sci USA. 2008;105(35):12815–9.

Wang H, Xu JZ, Zhu JJ, Chen HY. Preparation of CuO nanoparticles by microwave irradiation. J Cryst Growth. 2002;244(1):88–94.

Wang H, Oo Khor T, Shu L, Su Z, Fuentes F, Lee J-H, et al. Plants against cancer: a review on natural phytochemicals in preventing and treating cancers and their druggability. Anticancer Agents Med Chem. 2012;12(10):1281–305.

Wang JZ, Xiang JJ, Wu LG, Bai YS, Chen ZW, Yin XQ, et al. A genetic variant in long non-coding RNA MALAT1 associated with survival outcome among patients with advanced lung adenocarcinoma: a survival cohort analysis. BMC Cancer. 2017;17(1):167.

West JA, Davis CP, Sunwoo H, Simon MD, Sadreyev RI, Wang PI, et al. The long noncoding RNAs NEAT1 and MALAT1 bind active chromatin sites. Mol Cell. 2014;55(5):791–802.

Wilusz JE, Freier SM, Spector DL. 3′ End processing of a long nuclear-retained noncoding RNA yields a tRNA-like cytoplasmic RNA. Cell. 2008;135(5):919–32.

Xiang H, Kinoshita Y, Knudson CM, Korsmeyer SJ, Schwartzkroin P, Morrison RS. Bax involvement in p53-mediated neuronal cell death. J Neurosci. 1998;18(4):1363–73.

Yang XH, Sladek TL, Liu X, Butler BR, Froelich CJ, Thor AD. Reconstitution of caspase 3 sensitizes MCF-7 breast cancer cells to doxorubicin- and etoposide-induced apoptosis. Cancer Res. 2001;61(1):348–54.

Yang L, Lin C, Liu W, Zhang J, Ohgi KA, Grinstein JD, et al. NcRNA- and Pc2 methylation-dependent gene relocation between nuclear structures mediates gene activation programs. Cell. 2011;147(4):773–88.
Ye W, Xu P, Zhong S, Threlfall WR, Frasure C, Feng E, et al. Serum harvested from heifers one month post-zeranol implantation stimulates MCF-7 breast cancer cell growth. Exp Ther Med. 2010;1(6):963–8.
Yin C, Knudson CM, Korsmeyer SJ, VanDyke T. Bax suppresses tumorigenesis and stimulates apoptosis in vivo. Nature. 1997;79(7):1039–41.
Yin AJ, Li J, Jian W, Bennett AJ, Xu JM. Fabrication of highly ordered metallic nanowire arrays by electrodeposition. Appl Phys Lett. 2001;79(7):1039–41.
Zapata JM, Pawlowski K, Haas E, Ware CF, Godzik A, Reed JC. A diverse family of proteins containing tumor necrosis factor receptor-associated factor domains. J Biol Chem. 2001;276(26):24242–52.
Zhang Q, Li Y, Xu D, Gu Z. Preparation of silver nanowire arrays in anodic aluminum oxide templates. J Mater Sci Lett. 2001;20(10):925–7.
Zhao W, Luo J, Jiao S. Comprehensive characterization of cancer subtype associated long non-coding RNAs and their clinical implications. Sci Rep. 2014;4(1):1–7.
Zheng XG, Xu CN, Tomokiyo Y, Tanaka E, Yamada H, Soejima Y. Observation of charge stripes in cupric oxide. Phys Rev Lett. 2000;85(24):5170.
Zienolddiny S, Haugen A, Lie JAS, Kjuus H, Anmarkrud KH, Kjærheim K. Analysis of polymorphisms in the circadian-related genes and breast cancer risk in Norwegian nurses working night shifts. Breast Cancer Res. 2013;15(4):R53.

Publisher's Note

Springer Nature remains neutral with regard to jurisdictional claims in published maps and institutional affiliations.